Theses and Dissertations

6-30-2016

Ultra-High Temperature Full Field Deformation Measurements Of Materials Subjected To Thermo-Mechanical Loading: A DIC Based Study

Guillemo A. Valeri Paoli
University of South Carolina

Follow this and additional works at: http://scholarcommons.sc.edu/etd

Part of the Aerospace Engineering Commons

ULTRA-HIGH TEMPERATURE FULL FIELD DEFORMATION MEASUREMENTS OF MATERIALS SUBJECTED TO THERMO-MECHANICAL LOADING: A DIC BASED STUDY

by

Guillermo A. Valeri Paoli

Bachelor of Science
Universidad de Los Andes, 2013

Submitted in Partial Fulfillment of the Requirements

For the Degree of Master of Science in

Aerospace Engineering

College of Engineering and Computing

University of South Carolina

2016

Accepted by:

Addis Kidane, Director of Thesis

Michael Sutton, Reader

Lacy Ford, Senior Vice Provost and Dean of Graduate Studies

ACKNOWLEDGEMENTS

I would like to acknowledge Dr. Addis Kidane for his continued guidance and support throughout the duration of my graduate career. Thanks to his encouragement and advice, I have gained professional experience as an engineer.

Dr. Michael Sutton is acknowledge here for his advice on this work and for his position as reader and committee member for this thesis. I also thank my respected professors in the department of mechanical engineering for contributing to my academic preparation.

I would like to specially acknowledge Behrad Koohbor for his valuable help and guidance during my research and course work and particularly for his help in the VFM presented is this work.

This page would be incomplete without the mention of all members of Dr. Kidane's research group, for their recommendations and company throughout my research work and my friends and colleagues in mechanical engineering for their moral support and optimism towards my graduate career

Finally, I would like to express my gratitude towards my parents, my brothers, and my extended family and friends who have continuously motivated and supported me.

ABSTRACT

Determining the mechanical response of materials at elevated temperatures is a subject of great interest in metal forming, aerospace and aero-engine industries. For example, measurement of the deformation response under tensile loading at high temperatures is crucial for establishing thermomechanical and thermo-physical properties of materials, consequently, determining the reliability of a component or structure exposed to elevated temperatures. In order to predict the behavior of materials at ultra-high temperatures, a novel experimental approach based on Digital Image Correlation (DIC) is proposed and successfully applied to different materials at temperatures ranging from room temperature to 1100°C. In these studies, a portable induction heating device equipped with custom made water-cooled copper coils is used to heat the specimens. Two different illumination sources along with optical band-pass notch filters, and a stereo-camera configuration system is used to perform 3D-DIC to analyze stereo-images at a specific temperature.

The effectiveness of the system is demonstrated by successfully performing two different types of experiments; 1) to obtain the coefficient of thermal expansion (CTE) for two different materials, 309 stainless steel and titanium grade II, as a function of temperature, from room temperature to 1100 °C, 2) to study tensile response of a 304 stainless steel specimen subjected to quasi-static tensile

loading at temperatures between 300°C and 900°C. Numbers of experiments are conducted to study the sensitivity, spatial resolution and repeatability of the DIC measurements. The effect of heat haze on the measurement accuracy is also investigated for this method. Finally, using the temperature and load histories along with the full-field strain data, a Virtual Fields Method (VFM) based approach is implemented to identify the constitutive parameters governing the plastic deformation of the material at high temperatures.

Results from these experiments confirm that the proposed method can be used to measure the full field deformation of materials at ultra-high temperatures subjected to thermo-mechanical loading. Detailed experiment method, analysis and discussion will be presented.

TABLE OF CONTENTS

LIST OF TABLES

LIST OF FIGURES

CHAPTER 1
INTRODUCTION

1.1 DISPLACEMENT AND STRAIN MEASUREMENT

Surface deformation measurement of materials and structures subjected to mechanical and thermal loading is an important topic in the field of experimental solid mechanics. The importance of these experimental measurements at high temperature deformation is due to their significance in the full-field characterization of thermomechanical and thermophysical properties of various materials. These materials are used in high temperature applications such as aerospace industries, high temperature components in aeroengines, automotive, power generation, and high temperature material processes such as, surface treatments, alloying, coatings production, welding, cutting, melting, etc. [10]. The need for an accurate characterization of the mechanical behavior of materials at high temperatures has led to the development of numerous measurement methods. Aside from the widely used pointwise strain gauge technique, different full-field non-contact optical methods, such as speckle interferometry, moiré interferometry , and holography interferometry, and non-interferometric techniques, such as the grid method and digital image correlation (DIC), have been developed and applied for this purpose. However, interferometric metrologies are more difficult to implement, since they

require a coherent light source and the measurements need to be conducted in a vibration-isolated optical platform in the laboratory. Interferometric techniques measure the deformation of the specimen by recording the phase difference of the scattered light wave from the specimen surface before and after deformation. The measurement results are usually presented in the form of fringe patterns; consequently, further fringe processing and phase analysis techniques are required to obtain actual displacement results [8]. On the other hand, there have been efforts in the past two decades to improve non-interferometric full-field measurement techniques such as DIC in the analysis of the thermomechanical behavior of materials subjected to high temperature deformation [2].

1.2 DIGITAL IMAGE CORRELATION (DIC)

One of the earlier works in the field of image correlation was performed in the early 1950s by Gilbert Hobrough [9], who compared analog representations of photographs to register features from various views. Hobrough was able to design and construct an apparatus to correlate high-resolution reconnaissance photography in order to enable more precise measurement of changeable ground conditions, thus being one of the first investigators to perform image correlation. When digitalized images became more accessible in the 1960s and 1970s, investigators in robotics and artificial intelligence began to develop vision-based algorithms and stereo-vision methodologies in parallel with photogrammetry applications for aerial photographs. By then, digital image analysis was going

through an explosive growth, meanwhile, the field of experimental solid mechanics was focused on applying recently developed laser technology to measure deformation: holography, laser speckle, laser speckle photography, and interferometry techniques mentioned before. In 1983, Sutton et al. [1], developed numerical algorithms and performed preliminary experiments using optically recorded images. In the last decade, 2D-DIC has undergone an immense worldwide growth; there have been numerous articles using this method since the year 2000. 2D-DIC requires principally in-plane strains and displacements, and therefore, even small out-of-plane motions will introduce substantial errors in the deformation measurement. This signifies that 2D-DIC is applicable to plane surfaces only and not on curved surfaces, or the cases where substantial out-of-plane displacements occur. To resolve this problem, a stereovision system was developed and employed to make deformation measurements in the late 1990s [9].

Thanks to developments taken place in recent years, three-dimensional digital image correlation (3D-DIC) is now being used for a wide range of time-scales and length-scales. 3D DIC has been successfully implemented in applications such as: determining all three components of velocity of imaged fluid particles [11], the use of stereo optical microscopy for deformation and shape measurements on specimen dimensions ranging from a few 300 µm to a few millimeters [15, 20], high speed imaging systems for use in dynamic stress-strain response (shock loading) [13, 16, 17], measurement of shape and deformation on cylindrical surfaces [17], and fracture mechanics studies. [14, 16]. Material characterization has also been

an area of study for engineered materials like composites [12, 14, 16], and foams [17] or bio-materials such as biological tissues [18]. In addition, 3D-DIC has been applied on large scale models in civil engineering applications [19] and high temperature deformation measurements, as well [2 - 7]. In particular, high temperature deformation measurements based on optical methods has been a subject of great interest for the last two decades.

1.3 DIC FOR HIGH TEMPERATURE APPLICATIONS

Determining the material behavior and its properties at high temperatures is a subject of great interest in metal forming, aerospace and aero-engine industries. Measuring the strain and deformation response under tensile loading at high temperatures is crucial for establishing thermomechanical and thermophysical properties of materials, consequently, determining the reliability of a component or structure exposed to elevated temperatures.

DIC is probably one of the most appealing techniques for high temperature applications; it has various benefits compared to traditional methods that use externally applied extensometers, strain gauges or different non-contact optical methods to measure strain. DIC consists of a simple experimental setup with straightforward specimen preparation. It has the capability to adjust the spatial resolution, ability to take measurements on curved surfaces and different specimen sizes and/or shapes, and also the suitability for static and high speed measurements. By using DIC, the average data can be obtained from the full-field

data, while also, important local variations can be quantified at any area of interest on the surface; this is the case for heterogeneous materials or at surfaces where the temperature is not constant. It is also applicable to the study both, small and large deformations responses [9].

There have been studies where high temperature DIC was used to measure strains from room temperature up to 2600℃ [3]. The first work was performed by J. S. Lyons et al [2] in 1996. In this study, the authors conducted a series of experiments to assess the ability of DIC to measure full-field surface deformations at elevated temperatures. For this, a Lindberg furnace, a digital camera with 200 mm lens and white light illumination were used to study the free thermal expansion strains of an Incoloy 909 specimen and uniform tensile loading of an Inconel 718 specimen. Both specimens where speckled with special ceramic coatings and heated to a maximum temperature of 650℃. In this work, the authors found two sources of measurement error that caused image distortion: 1. the furnace window, and 2. variations in the refractive index of heated air outside the furnace. The first problem was solved using an optical quality sapphire furnace window instead of the standard sapphire window supplied with the furnace. The second problem was solved by implementing a small fan near the furnace window blowing air perpendicular to the camera's focal axis. The fan mixed the air such that the air temperature remained constant, not affecting the index of refraction and eliminating the distortion of the specimen's image. By plotting the strain vs temperature, the coefficient of thermal expansion (CTE) was determined. The technique showed good agreement between the CTE values measured and the

5

values calculated. Finally, tension tests were performed using a dead-weight lever-arm system deforming the Inconel 718 specimen with in the elastic region. The results of this work indicated that DIC is capable of measuring thermal and mechanical strains at elevated temperatures (650 ℃) with the same level of accuracy as in ambient temperature.

Another limitation found on high temperature DIC, is the visible thermal radiation emitted by the material when heated to temperatures above 650-700 ℃, which is brighter than the light source. This black-body radiation alters the contrast within the surface features (speckles) and makes them very difficult to be interpreted by the correlation routine. The authors [2] suggest using brighter light and/or filtering the appropriate wavelengths of radiation to allow accurate measurements at higher temperatures.

Black-body radiation is described by Planck's equation as a function of temperature and wavelength.

$$I(\lambda, T) = \frac{2hc^2}{\lambda^5} \frac{1}{e^{\frac{hc}{\lambda kT}} - 1} \qquad (1)$$

Where, $I(\lambda, T)$ is the thermal radiation energy or intensity, h is Planck's constant, c is the speed of light, and k is the Boltzmann constant and e is the Euler's number. By plotting the radiation energy as a function of wavelengths and temperatures ranging from 200 to 1200 ° C, one can observe that as temperature rises, the emitted thermal radiation includes shorter wavelengths and the radiation increases rapidly, see next figure.
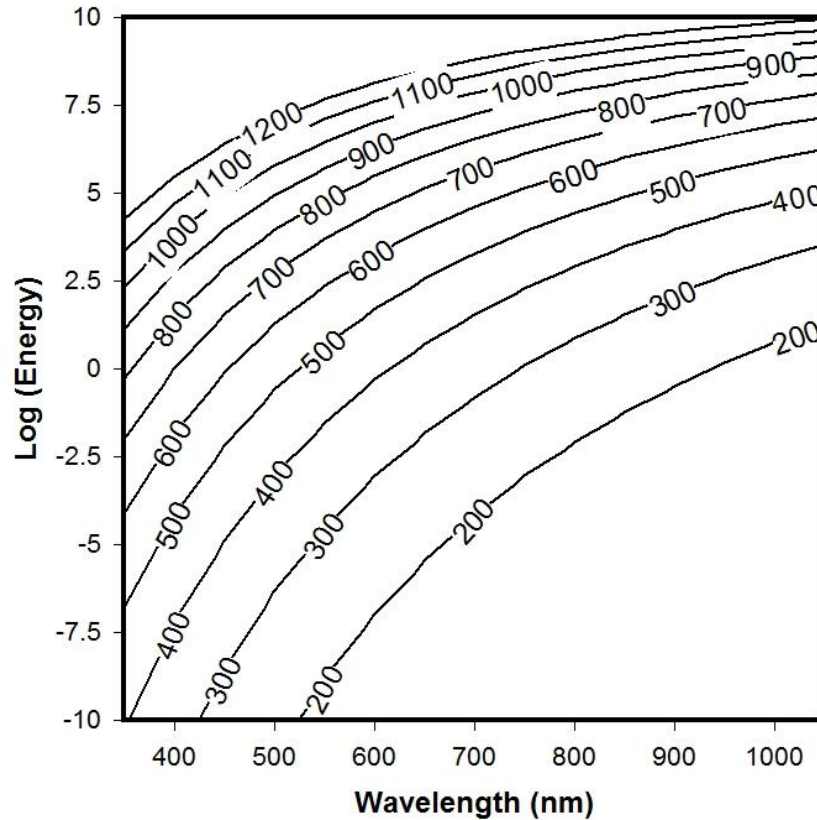
Figure 1.1. Thermal radiation energy as a function of wavelength at various temperatures

Recent works have studied DIC for measuring strains at temperatures ranging from room temperature to 1200℃. Grant et al [4] presented a method that overcomes the black body radiation issue by the implementation of optical filters and special illumination, providing accurate DIC measurements up to 1100℃. The experiment consisted of a nickle-based superalloy (RR1000) specimen, with no applied speckle pattern. The material was loaded under tension and high temperatures, and the Young's Modulus and CTE were measured. The sample heating was accomplished by ohmic heating from a current applied across the sample with feedback control from a thermocouple attached to the sample, and

images taken by one 4M CCD camera. The system required an environmental chamber to reduce the oxidation by protecting the sample in an argon atmosphere. The results obtained in this work were found to be consistent with values reported by Rolls-Royce plc (RR1000). Grant et al. [4] also found that at temperatures exceeding 800 ℃, the level of measurement accuracy is deteriorated due to a rapid oxidation rate. To overcome this issue, the authors proposed the application of a vacuum chamber for future works. Heat haze was not found to be a problem in this work [4].

Another limitation associated with the application of DIC at high temperatures is the deteriorating effect of extreme high temperatures to the speckles on the surface of the specimen. In recent years, the application of novel speckling methods capable of sustaining integrity and efficiency at extreme temperatures has been studied. Authors have used high temperature resisting coatings, such as LSI boron nitride and aluminum oxide-based ceramic coatings [2], temperature resistant white Y2O3 paint and other ceramic paints [6], a blend of black cobalt oxide with liquid commercial inorganic adhesive [5] to form the speckle. Other studies implemented greater resistance techniques, such as using plasma spray for specimen preparation [3], where sprayed tungsten powder was employed at temperatures up to 2600 ° C, and finally, the use of the material's natural texture as speckle patterns for correlation [4 and 7].

More research is needed to study a simpler high temperature DIC technique for material characterization that overcomes the previously described limitations, and employs a portable heating system that is compatible with multiple testing

8

machine configurations and for different sample size and geometries, to take advantage of the convenience of the DIC's simple and versatile setup equipment.

1.4 OBJECTIVE

The present work focuses on the application and study of a portable novel 3D DIC high temperature measurement system that can be employed on a wide range of specimen geometries and sizes. In Chapter 2, the experimental methodology, equipment, set up and software used in the experiments are described. Chapter 3 describes the study and analysis of a specimen subjected to high temperature free expansion, where High temperature DIC limitations, sensitivity, spatial resolution, and distortion are studied for two different illumination conditions. The effectiveness of the system is also verified by successfully conducting experiments at temperatures up to $1150°C$ and $1000°C$ on a 309 stainless steel and titanium specimen, respectively, to determine the variation of the coefficient of thermal expansion (CTE) as a function of temperature. In Chapter 4 the same portable heating devise is used along with a tensile test machine to study the thermomechanical properties of a stainless steel 304 specimen, using a novel high temperature speckle technique, blue light LED illumination and a band pass optical filter for image acquisition at temperatures ranging from room temperature ($25°C$) up to $900°C$. Finally, the full-field surface measurement results from the experiments were used along with the Virtual Fields Method to identify the visco-plastic constitutive response of the examined material.

LIST OF REFERENCES

[1] M.A. Sutton, W.J. Wolters, W.H. Peters, W.F. Ranson and S.R. McNeill, 1983, "Determination of Displacements Using an Improved Digital Correlation Method," Image and Vision Computing, **1(**3), pp. 133-139.

[2] J. S. Lyons, J. Liu, and M. A. Sutton, 1996, "High-temperature Deformation Measurements Using Digital-image Correlation," Experimental Mechanics, **36**(1), pp. 64-70.

[3] X. Guo, J. Liang, Z. Tang, B. Cao, and M. Yu, 2014, "High-Temperature Digital Image Correlation Method for Full-Field Deformation Measurement Captured with Filters at 2600∘C using Spraying to Form Speckle Patterns," Optical engineering, **53**(6), pp. 063101-1-12.

[4] B. Grant, H. Stone, P Withers, and M. Preuss, 2009, "High-Temperature Strain Field Measurement using Digital Image Correlation," Journal of strain analysis for engineering design, **44**(4), pp. 263-271.

[5] B. Pan, D. Wu, Z. Wang, and Y. Xia, 2011, "High-Temperature Digital Image Correlation Method for Full-Field Deformation Measurement at 1200∘ C," Measurement Science and Technology, 22, pp. 015701-1-11.

[6] B. Koohbor, G. Valeri, A. Kidane, M. Sutton, 2015, "Thermo-Mechanical Properties of Metals at Elevated Temperatures," Advancement of Optical Methods in Experimental Mechanics, **3**, pp. 117-123.

[7] H. Su, X. Fang, Z Qu, C. Zhang, B. Yan, and X. Feng, 2015, "Synchronous Full-Field Measurement of Temperature and Deformation of C/SiC Composite Subjected to Flame Heating at High Temperature," Experimental mechanics, DOI 10.1007/s11340-015-0066-5.

[8] Bing P, Kemao Q, Huimin X and Anand A, 2009, "Two-Dimensional Digital Image Correlation for In-Plane Displacement and Strain Measurement: a Review," Measurement Science and Technology, **20**(6), pp. 062001-1-17.

[9] M A. Sutton, J J. Orteu and H W. Schreier, 2009, *Image Correlation for Shape, Motion and Deformation Measurements*, Springer. New York, NY.

[10] Yang Y, Li X, Xiao R and Zhang H, 2015, "Digital Image Correlation and Complex Biaxial Loading Tests on Thermal Environment as a Method to Determine the Mechanical Properties of Gh738 using Warm Hydroforming," High Temperature Material Processes, **19**(1), pp. 37-69.

[11] K. D. Hinsch and H. Hinrichs, 1996, "Three-dimensional Particle Image Velocimetry," Three-Dimensional Velocity and Vorticity Measuring and Image Analysis Techniques, **4,** pp. 129-152.

[12] V.P. Rajan, M.N. Rossol and F.W. Zok, 2012, "Optimization of Digital Image Correlation for High-Resolution Strain Mapping of Ceramic Composites," Experimental Mechanics, **52**(9), pp. 1407-1421.

[13] F. Pierron, M.A. Sutton and V. Tiwari, 2011, "Ultra High Speed DIC and Virtual Fields Method Analysis of a Three Point Bending Impact Test on an Aluminum Bar," Experimental Mechanics, **51**(4), pp. 537-563.

[14] B. Koohbor, S. Mallon, A. Kidane and M. A. Sutton, 2014, "A DIC-Based Study of In-Plane Mechanical Response and Fracture of Orthotropic Carbon Fiber Reinforced Composite," Composites Part B: Engineering, **66**, pp. 388–399.

[15] B. Koohbor, S. Ravindran and A. Kidane, 2015, "Meso-Scale Strain Localization and Failure Response of an Orthotropic Woven Glass-Fiber Reinforced Composite," Composites Part B: Engineering, **78**, pp. 308–318.

[16] S. Mallon, B. Koohbor, A. Kidane and M.A. Sutton, 2015, "Fracture Behavior of Prestressed Composites Subjected to Shock Loading: A DIC-Based Study," Experimental Mechanics, **55**(1), pp. 211-225.

[17] B. Koohbor, A. Kidane, W. Lu and M.A. Sutton, 2016, "Investigation of the Dynamic Stress–Strain Response of Compressible Polymeric Foam Using a Non-Parametric Analysis," International Journal of Impact Engineering, **91**, pp. 170–182.

[18] D. Zhang and D.D. Arola, 2004, "Applications of Digital Image Correlation to Biological Tissues," Journal of Biomedical and Optics, **9**(4), pp. 691-699.

[19] R. Ghorbani, F. Matta and M.A. Sutton, 2015, "Full-Field Deformation Measurement and Crack Mapping on Confined Masonry Walls Using Digital Image Correlation," Experimental Mechanics, **55**(1), pp. 227-243.

[20] M.A. Sutton, N. Li, D.C. Joy, A. P. Reynolds and X. Li, 2007, "Scanning Electron Microscopy for Quantitative Small and Large Deformation Measurements Part I: SEM Imaging at Magnifications from 200 to 10,000," Experimental Mechanics, **47**(6), pp. 775-787.

CHAPTER 2
EXPERIMENTAL METHOD

2.1 INTRODUCTION

Before studying the tensile response of materials subjected to high temperatures using DIC, an analysis of this technique and its effectiveness under elevated temperature conditions is necessary. To do so, experiments were performed where the specimen was continuously heated to 1100 °C under two different illumination conditions: blue and white light. As mentioned in the objective, a sensitivity analysis was performed, where the specimen was subjected to free expansion and 10 images were obtained at different step temperatures and statistically analyzed to determine noise, spatial resolution, distortion and other limitations of this method. The main objective of this experiment was to construct continuous strain vs temperature plots, calculate the CTE and compare the results using blue and white light with the literature CTE values for two different materials. This comparison will state the effectiveness of this technique. Also, a test was performed to study the effect of heat haze in the current experimental setup. Finally, the same experimental setup along with a tensile testing machine, was used to study the high temperature tensile response of the specimens and determining its properties using blue light illumination and a band pass optical filter

at temperatures ranging from room temperature up to 900℃. A sensitivity analysis was also performed for this set up.

2.2 EQUIPMENT USED

All the tests performed in this work were accomplished using the same equipment and software. However, different materials were employed with different specimen shape and dimensions.

Heating Source:

Specimens were heated using an Across International IH15 Series Induction Heater [1] equipped with custom-made water-cooled copper coils. The induction heating system is a portable table-top unit suitable to heat up a wide variety of specimen geometries and sizes and can be employed with different testing machines, as long as it is equipped with an appropriate coil system. The following table shows the characteristics of the induction heater used in this study.

Table 2.1. Induction heater system characteristics

Input Voltage	220 VAC single phase
Output Frequency	20 – 80 KHz (mid frequency)
Heating Current	200 – 600 A
Heating Rate used	≈ 1.6℃ / sec
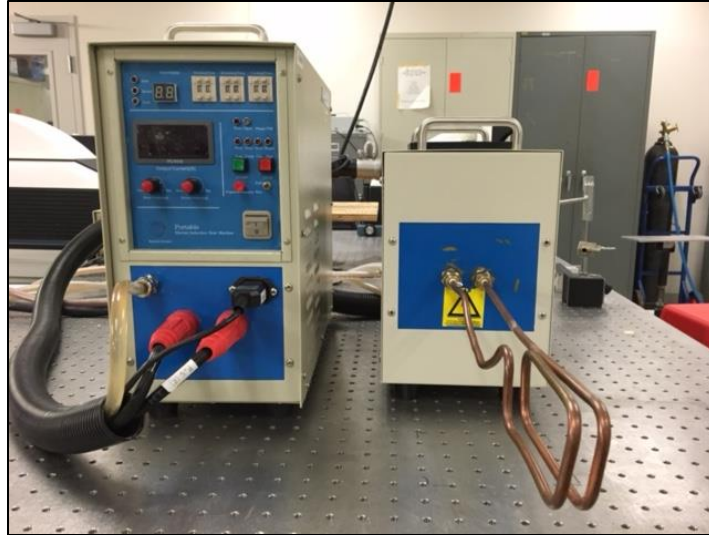
Figure 2.1. Portable induction heater

Water Chiller

The induction heating system is cooled by an Across International Industrial Water Chiller that is in charge of maintaining the water that flows through the induction coil at no more than $30\,^\circ$C. The chiller also cools the power supply and capacitor of the induction heating system.

Figure 2.2. Industrial water chiller

Thermometer

The temperature of the specimen was continuously measured using a non-contact infrared thermometer facing the center of the specimen, with an accuracy of $\pm3\,^\circ$C. The thermometer has a USB port and was connected to a computer to record the data.

Figure 2.3. CEM Infrared Thermometer

Cameras

A system of two 5 MP Point Grey® stereovision cameras [2] with 100 mm lenses were used to acquire the images for correlation. The following table shows the specifications of the camera model used.

Table 2.2.Cameras specification table

Model	GRAS-50S5M-C
Resolution	2448 x 2048
Frame Rate	15 FPS
Megapixels	5.0 MP
Chroma	Mono
Sensor Type	CCD
Pixel Size	3.45 µm
Exposure Range	0.02 ms to >10 seconds
Power Requirements	8 to 30 V
Operating Temperature	0 to 40˚C

Figure 2.4. Point Grey 5 MP cameras [2]

Optical Filter

It was previously mentioned that the grey-scale intensity of the images will experience a significant change at temperatures above 650 - 700 ˚C. This can be shown by plotting once again the radiation energy vs temperature at different wavelengths using Planck's equation (1). In the next figure, it is noticeable a remarkable increase in the magnitude of radiation energy as temperature increases beyond T ≈ 700oC. However, the rate of change of the radiation energy is significantly lower for 450 nm wavelengths than for the other two. This demands

17

for the use of band pass optical filters which allows shorter wavelengths, and also, additional illumination in order to minimize the unwanted change of grey-scale intensity and increase the level of accuracy in the DIC measurements.
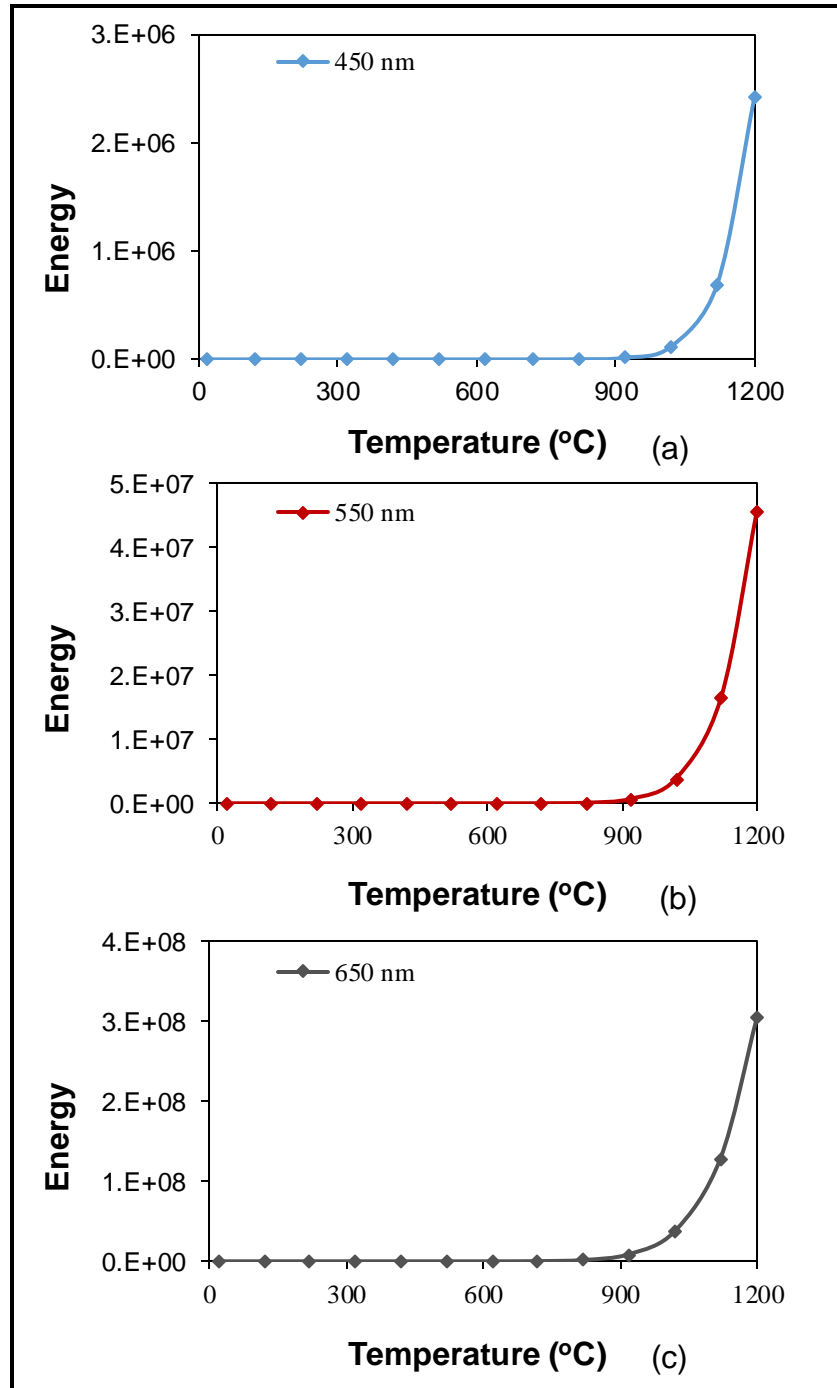
Figure 2.5. Variation of radiation energy with respect to temperature for optical wavelengths of (a) 450 nm, (b) 550 nm and (c) 650 nm

Consequently, two blue band pass optical filters [3] with a wavelength range of 435-495 nm were selected and employed in this work. The specifications of the selected filter are shown in the next table and figures.

Table 2.3. Technical characteristics of BP470-55 Blue Bandpass Filter [3]

Wavelength Range	425 – 495 nm
FWHM	85 nm
Tolerance	+/- 10 nm
Minimum Peak Transmission	> 90%
Surface Quality	40 /20
Compatible LED	450nm, 465nm, 470nm
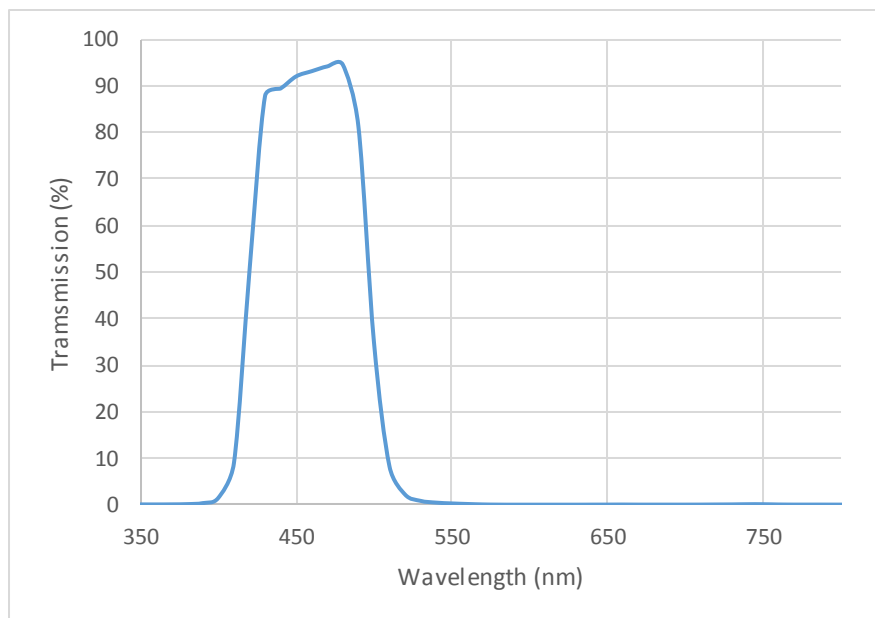
Figure 2.6. BP470 blue bandpass filter wavelength transmission range
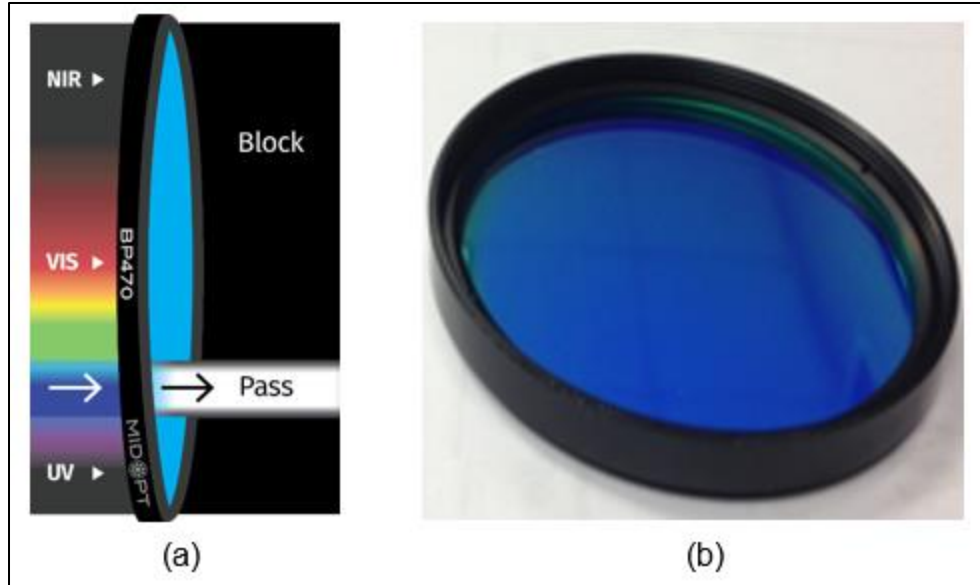
Figure 2.7. (a) Schematic figure of light filtering [3]. (b) Actual optical filter used

Illumination Source

Two different illumination systems were used: high intensity blue and white LED illumination.
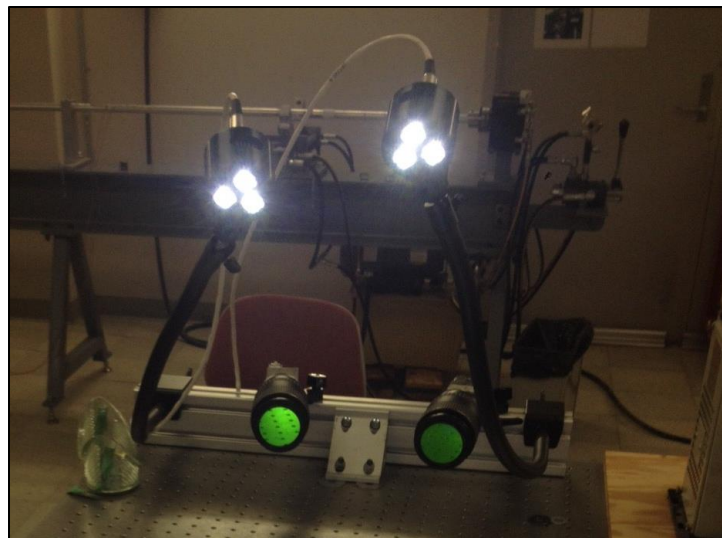
Figure 2.8. White light illumination set up

Tensile Testing Machine

Tensile tests were conducted using a Tinius Olsen 5000 tensile testing machine with a load cell of 20,000 N max load. The tests were performed in displacement control mode and at a constant cross head speed of 10 mm/min, which is equivalent to a mean strain rate of 2×10^{-3} s^{-1}.

Figure 2.9. Tinius Olsen 5000 tensile testing machine

Specimens Characteristics

In this work, three different materials were studied. Two of them, under free thermal expansion at elevated temperatures, and one, under tensile loads at

elevated temperatures. The first DIC measurements were performed using a rectangular fully annealed 309 stainless steel specimen. This material was selected due to its non-magnetic and superior scaling resistance characteristics.

Table 2.4. Stainless steel 309 chemical components [4]

Component	Wt. %
Carbon	Max 0.2
Chromium	22 – 24
Iron	Balance
Manganese	Max 2
Nickel	12 – 15
Phosphorus	Max 0.045
Silicon	Max 0.75
Sulphur	Max 0.03

A Titanium grade II rectangular specimen was also studied using DIC at high temperatures. This material is widely used in airframe components, cryogenic vessels and heat exchangers. It is composed of the following elements.

Table 2.5. Titanium grade II chemical components [5]

Component	Wt. %
C	Max 0.1
Fe	Max 0.3
H	Max 0.015
N	Max 0.03
O	Max 0.25
Ti	99.2

Both materials (309 SS and Titanium) were cut to the same size using a waterjet CNC cutting machine. Two 8mm holes were cut at the edges of the specimens in order to mount them inside the induction coil using two slimmer ceramic rods to allow their free expansion. The next figure shows the dimensions of the 309 stainless steel and titanium specimens
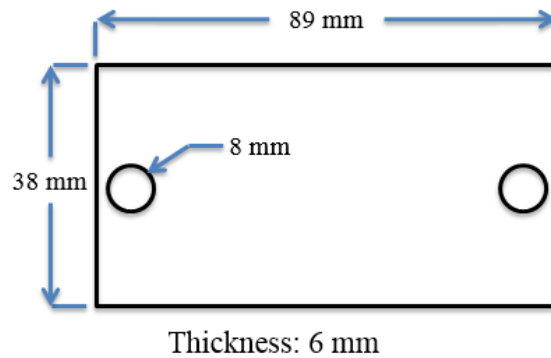
Figure 2.10. Stainless steel and titanium specimen dimensions for free expansion tests

Finally, low carbon 304 stainless steel flat dog-bone specimens were evaluated under high temperature tensile loading conditions and studied using DIC. It is composed of the following elements.

Table 2.6. Stainless steel 304 L chemical components [6]

Component	Wt. %
Carbon	Max 0.3
Chromium	18 – 20
Manganese	Max 2
Nickel	8 – 12
Phosphorus	Max 0.045
Silicon	Max 1
Sulphur	Max 0.03

The as-received stainless steel sheets were cut using a CNC waterjet to the dimensions showed in the following figure and table.
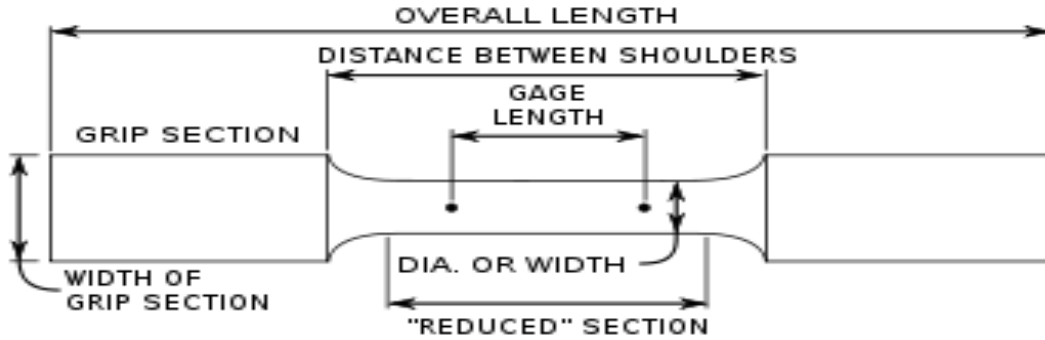
Figure 2.11. Flat dog-bone specimen dimensions

Table 2.7. Flat dog-bone specimen dimensions corresponding to Figure 2.11

Width	12. mm (0.5 in)
Approx. gage length	88 mm (3.46 in)
Thickness	3.18 mm (0.125 in)
Fillet radius	6.35 mm (0.25 in)
Overall Length	203.2 mm (8 in)

Figure 2.12. 304 Stainless steel flat dog-bone specimen cut using a CNC water jet

Speckle Pattern

All the specimens were coated with a thin layer of ultra-high temperature resistant white Yttrium Oxide spray paint (max temp: 1500°C). A high temperature silica-based ceramic paint was then applied on top of the white coating, obtaining a fine black speckle pattern. The specimens are kept at room temperature to let the paint fully dry for 24 hours. A typical speckled pattern used is shown in Figure 2.13.

Figure 2.13. Typical high temperature resistant speckle pattern used

Software

Various software packages were used in thus study: Vic-snap was used to obtain the images from the stereovision camera system. This program was synchronized with the infrared thermometer program in order to record one temperature measurement per image taken. The DIC software Vic-3D® [7] was

used to correlate the images and obtain the strains in the area of interest. Finally, other mathematic tools, such as Matlab, were used to analyze the data and construct the graphs and tables.

2.3 EXPERIMENTAL PROCEDURES

The first experiment type was a sensitivity analysis applied to a 309 stainless steel specimen [8]. For this, the speckled rectangle shaped specimen was held by the two ceramic rods inside the induction coil. Ten images were captured at room temperature before starting the heater. At that moment, the induction heater was turned on, and heated the specimen until it reached a maximum temperature of 1000˚C. Ten images were acquired at this temperature and the heater was turned off after a few seconds. As the specimen was cooling down evenly, 10 images were taken every 200 degrees: 1000, 800, 600, 400, 200˚ C. This same procedure was done using two illumination conditions, blue and white light. Each experiment was also repeated using a small table fan blowing air perpendicular to the cameras' focal axis in order to study the effect of heat haze. Further details of the sensitivity analysis will be described in Chapter 3. In order to calculate the coefficient of thermal expansion, the specimen was once again heated at a constant rate of 1.6˚C/sec, temperature data and images were taken every 2 seconds (0.5 Hz) until the specimen's center reached a temperature of 1150 ˚ C and 1000 ˚ C for the 309 stainless steel and titanium specimen, respectively. The next figure illustrates this experimental set up.

26
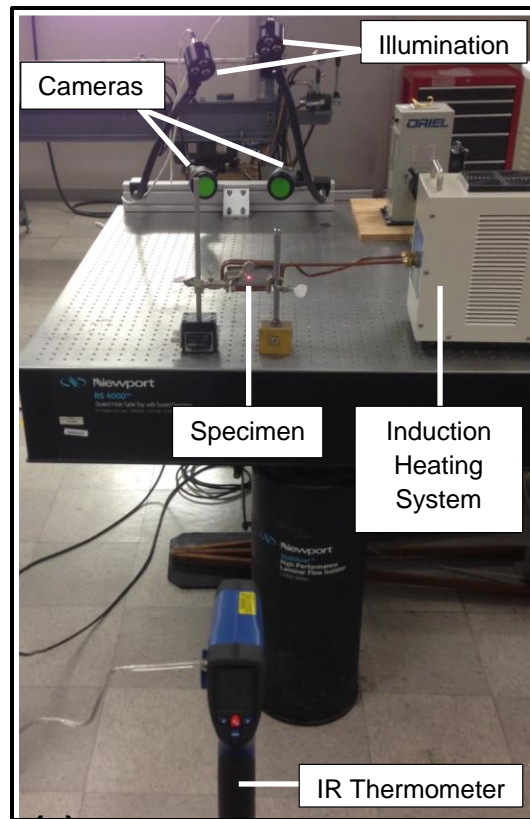
Figure 2.14. Experimental setup used for the CTE calculation tests

Finally, the same experimental setup, along with a tensile testing machine, was used to study the high temperature tensile response of a speckled flat dog-bone 304 stainless steel specimen and determining its properties. First, the tests were performed at room temperature (RT) to obtain the reference stress-strain response of the material using a displacement control mode tensile machine with a constant cross-head speed of 10mm/min. The tensile load is then converted to true stress. The high temperature tensile tests were performed on a similar manner: The specimen was clamped at the bottom grip of the tensile machine, inside the coil, and heated up to the target temperature, and after waiting several

minutes for the temperature to become uniform in the area of interest, the specimen was clamped at the top grip and the experiment immediately initiated (image, load and temperature data acquisition). This test was performed at RT, 300, 500, 700, and 900°C, using blue light illumination. The temperature history of the sample at the area of interest was synchronized to record at the same rate as the load and image acquisition. A sensitivity analysis was also performed for this test set up. This experimental procedure and its parameters are described in chapter 4 of this thesis. The next figure illustrates this experimental set up.
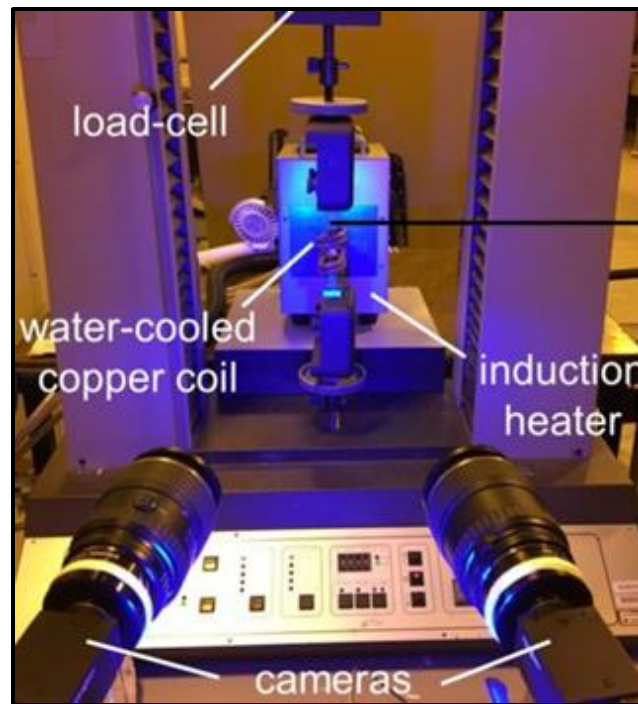
Figure 2.15. Experimental setup for high temperature tensile tests

LIST OF REFERENCES

[1] Across International, n.d., from http://www.acrossinternational.com

[2] Point Grey, n.d., from http://www.ptgrey.com

[3] Midwest Optical Systems, n.d., from http://www.midopt.com

[4] AK Steel, n.d., from http://www.aksteel.com

[5] Aerospace Metals, n.d., from http://www.aerospacemetals.com

[6] North American Stainless Steel, n.d., from http://www.northamericanstainless.com

[7] Correlated Solutions, n.d., from http://www.correlatedsolutions.com

[8] B. Koohbor, G. Valeri, A. Kidane, M. Sutton, 2015, "Thermo-Mechanical Properties of Metals at Elevated Temperatures," Advancement of Optical Methods in Experimental Mechanics, **3**, pp. 117-123.

CHAPTER 3
FREE EXPANSION TEST

3.1 INTRODUCTION

The free expansion experiments were performed for two different materials: 309 stainless steel and titanium grade II. Both specimens were tested using the same equipment and procedure. Chapter 3 describes in detail the analysis, results and conclusions of two types of experiments: A sensitivity analysis for the stainless steel specimen and the calculation of the coefficient of thermal expansion (CTE) of both materials. When performing these two experiments it is necessary to ensure the specimen is free to expand with no constraints, otherwise, a significant internal stress may be produced by the constraints affecting the strain measurement and ultimately throwing erroneous results. For this, the speckled rectangle shaped specimen was held by two ceramic rods inside the induction coil which allows the specimen to expand freely in all directions.

3.2 SENSITIVITY ANALYSIS

In order to study the accuracy of the strain measurement at high temperatures a sensitivity analysis or quantitative error analysis was performed. Ten images were taken at different step temperatures (25, 200, 400, 600, 800 and

1000°C) using white light and blue light separately, and also with fan and with no fan, as mentioned in the previous chapter. The analysis was performed in a 5 mm diameter circular area in the center of the specimen. The average strains were calculated in the circular area for each of the 10 images on all the step temperatures. Finally, the strains of the 10 images were averaged and the standard deviation was calculated to visualize the error in the measurement and compare it for all the temperatures. This same procedure was made for both illumination cases and with fan and no fan, to study the heat haze phenomenon. The following figure shows the 5 mm circular area of study in the center of the specimen and also compares the speckle pattern at room temperature with the same at 1000°C.
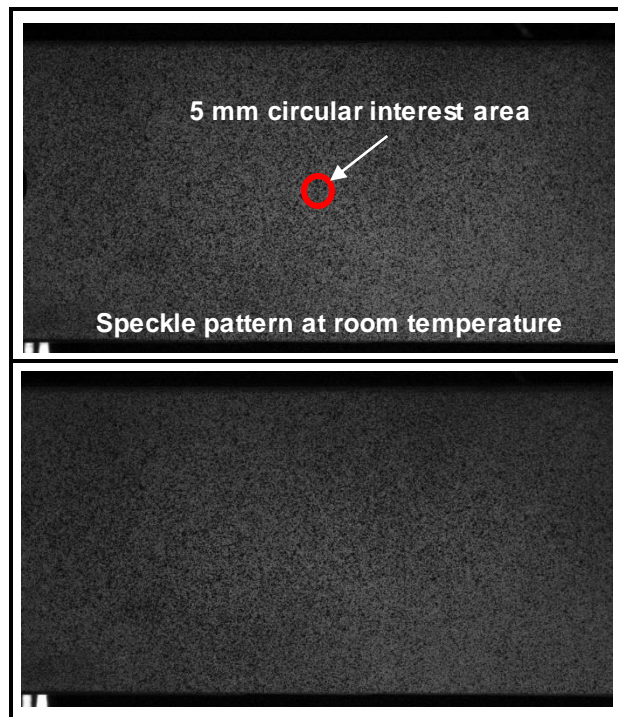
Figure 3.1. Specimen at lowest and highest temperature showing the speckle pattern and the 5 mm circular area of study
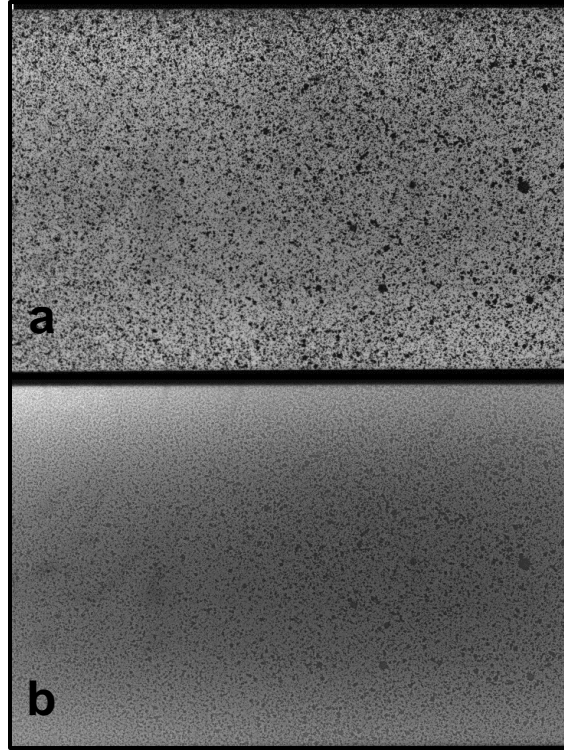
Figure 3.2. Comparison of the speckle pattern with (a) and without the optical filter (b)

The following figure shows a typical strain measurement in temperature steps, 10 images per temperature.
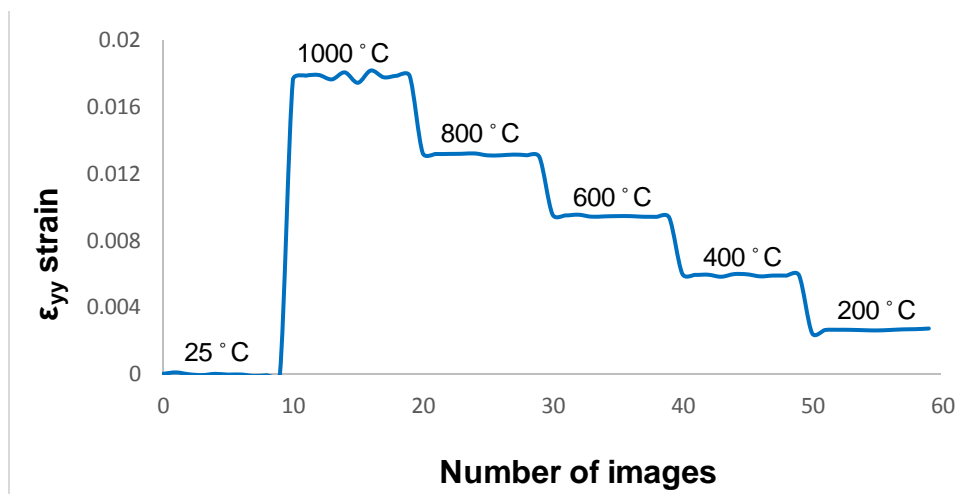
Figure 3.3. Typical sensitivity analysis experiment

It is noticeable in the previous figure that the images were taken during the cooling phase. The strain in the Y direction is greater at higher temperatures and almost constant at each temperature. The images were used as the input to the DIC software using a subset of 33 pixels and a step size of 11 pixels. The spatial resolution was calculated to be 26 µm/pix. The next figures show the average strain and standard deviation of the ten images taken at each temperature using different ilumination and ventilation conditions.
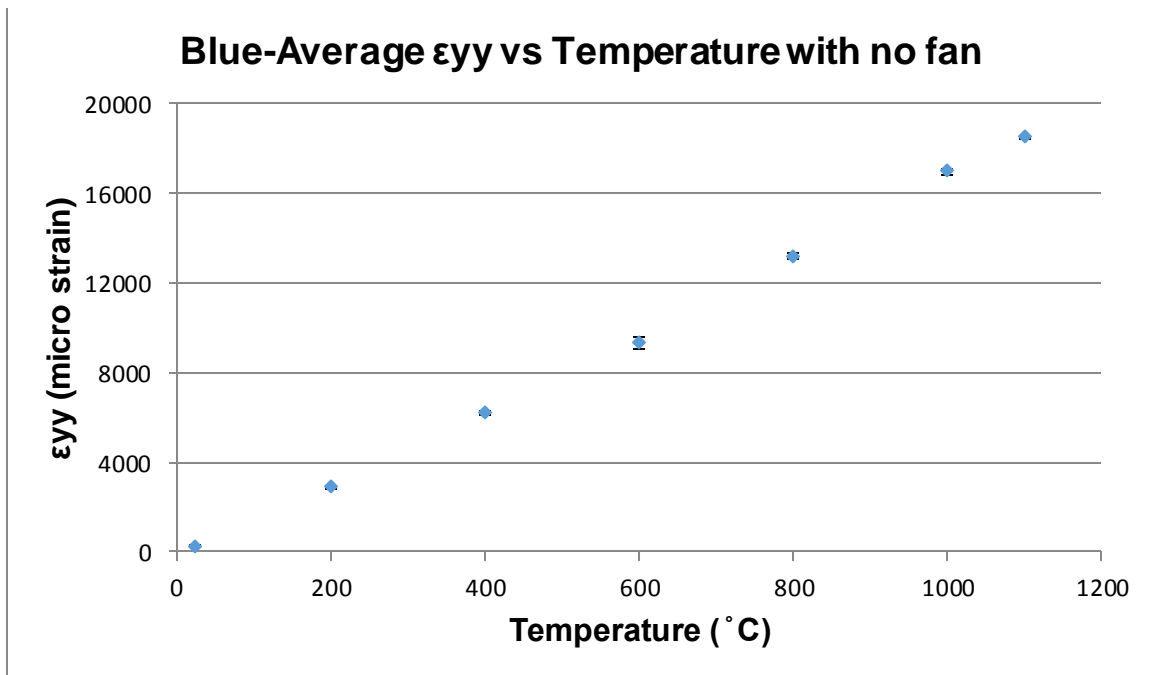
Figure 3.4. Strain vs temperature under blue light illumination and no fan
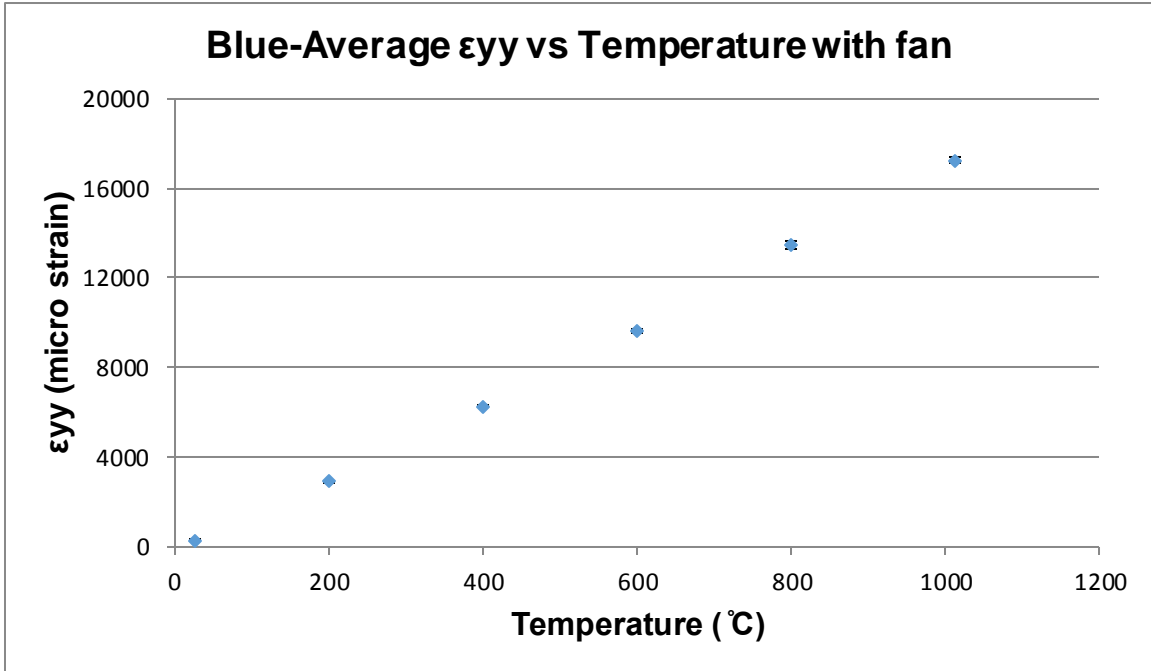
Figure 3.5. Strain vs temperature under blue light illumination with fan
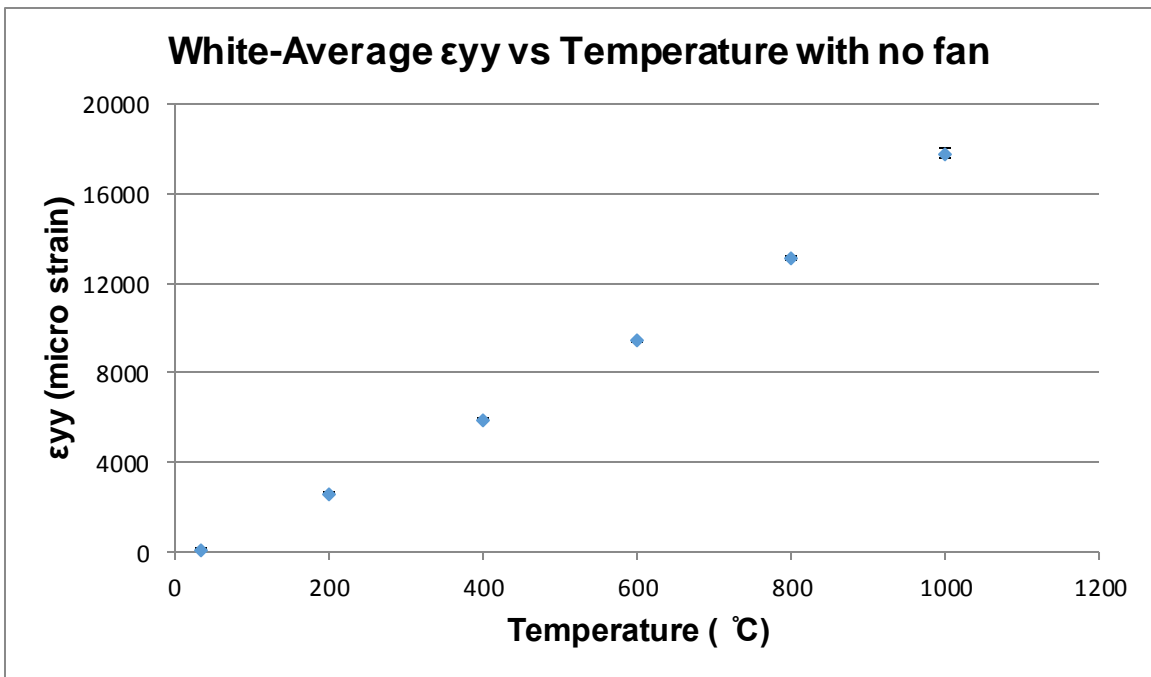
Figure 3.6. Strain vs temperature under white light illumination and no fan
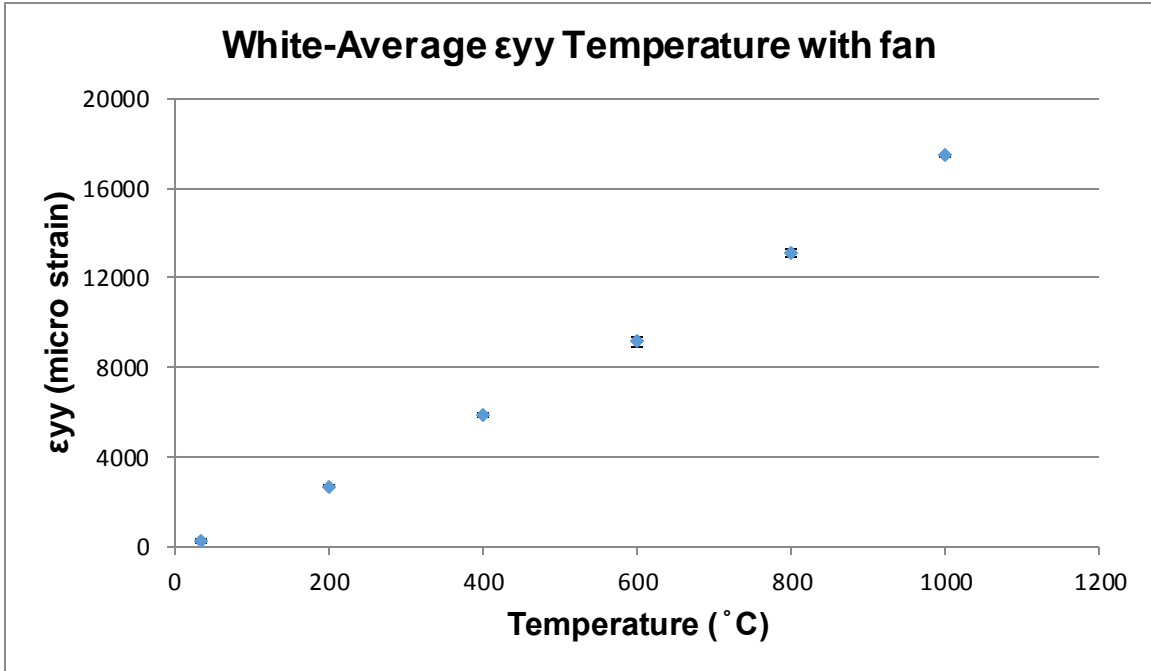
Figure 3.7. Strain vs temperature under white light illumination with fan

Figure 3.4 to Figure 3.7, show the results of the analysis for the different conditions. For all cases (blue light, white light, with fan and no fan), a SD of < 3% of the micro strain was found between the 10 images taken at each temperature; this indicates the high level of accuracy in the strain measurements of this technique. It is also demostrated that with the use of a blue band pass optical filter, high quality images can be obtained at temperatures up to 1,100 $^{\circ}$C, with the use of either: white light as well as blue light. No specific trend was found that requires a specific illumination source other than white light. Similarly, it is also conlcuded that heat haze is not an issue for this experimental set up. The implementation of a fan did not show any improvement or trend in the results; this is due to the fact that there is no enclosed enviromental chamber in this setup. Figure 3.8 compares the standard deviation versus temperature for all conditions.

In general, it is noticeable a small increment of SD as the temperature increases, however the increase is insignificant. In conclusioin, no particular trend is observed for white or blue illumination and/or with and without the use of a fan.
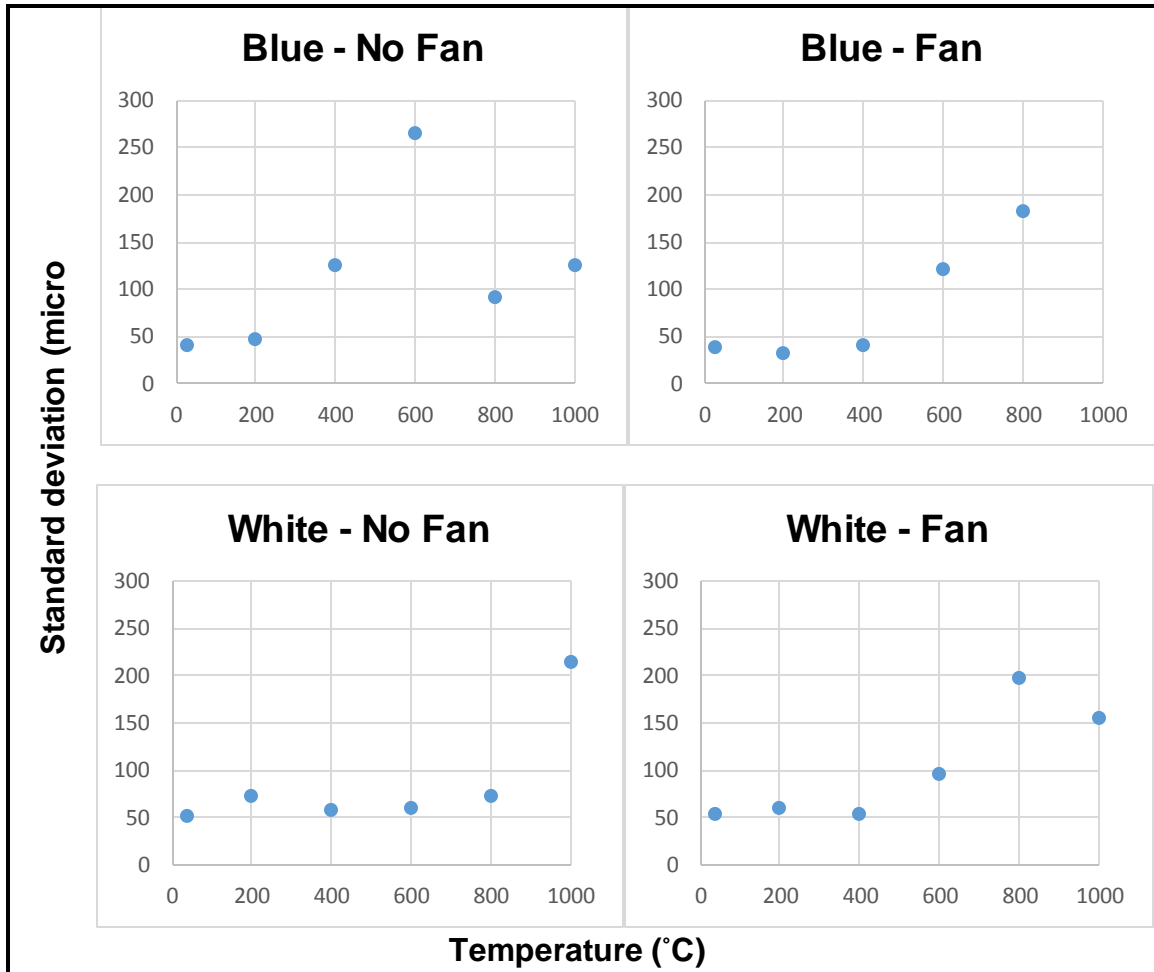
Figure 3.8. Micro strain in the vertical axis vs temperature. Comparison for all tested conditions

3.3 CALCULATION OF THE COEFFICIENT OF THERMAL EXPANSION

Displacement (u and v) full-field contours at different temperatures of the 309 stainless steel specimen, using blue light illumination, are shown in the next

36

figure. This images were taken during the continuous cooling phase of the specimen every two seconds along with the temperature measurements, and correlated using the same parameters as in section 3.2. Only three temperatures are shown. It is noticeable that the in-plane rigid body motion of translation and rotation, has been eliminated. Consequently, an equally spaced pattern for horizontal and vertical displacements is clearly demonstrated. The displacement patterns in the figure, including the displacement magnitude contours, also indicate a homogeneous thermal expansion.
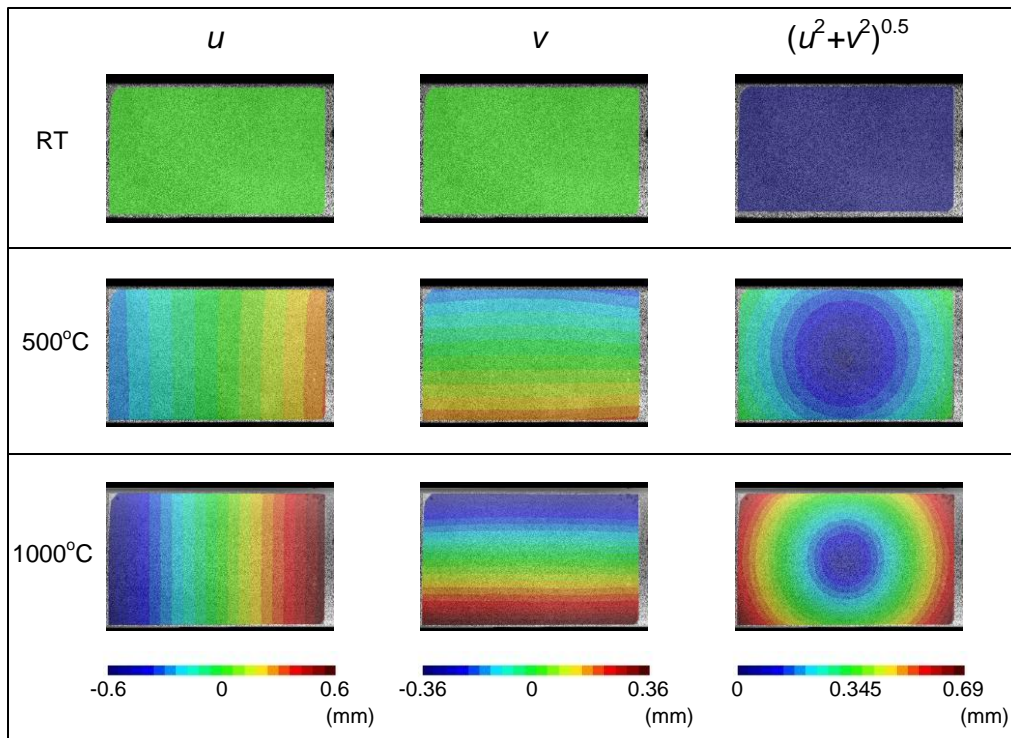
Figure 3.9. Full-field vertical and horizontal displacement contours using blue light source

Similarly, the strain contours were also plotted and studied. The next figure demonstrates the horizontal and vertical (ε_{xx} and ε_{yy}) full-field strain components

37

using the blue illumination condition. It is noticeable a remarkably homogeneous distribution of both strains. Also, it is observed that the averaged values of ε_{xx} and ε_{yy} over the entire area of interest, are very similar at 1000°C (ε_{xx} = 0.0192±2% and ε_{yy} = 0.0185±2%), this demonstrates the material's isotropic free thermal expansion response.
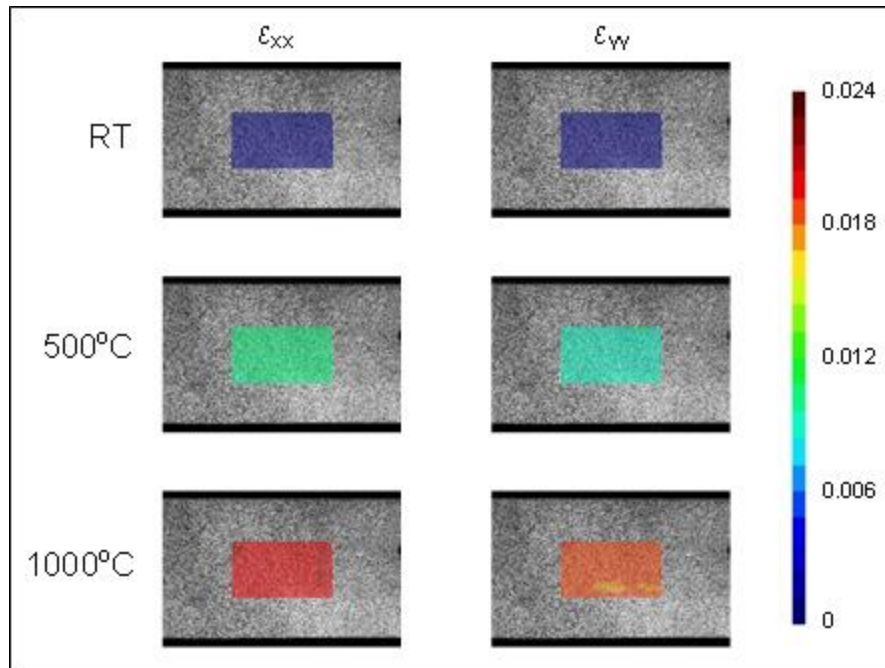
Figure 3.10. Horizontal and vertical shear full-field contours at room temperature (RT), 500 and 1000°C, using blue light conditions

Finally, strain vs temperature curves were constructed for both illumination conditions using data within the center point of the specimen. This graphs were made using data from 309 stainless steel and titanium specimens, during the cooling phase, from 1150°C and 1000°C, respectively, down to room temperature (25°C).
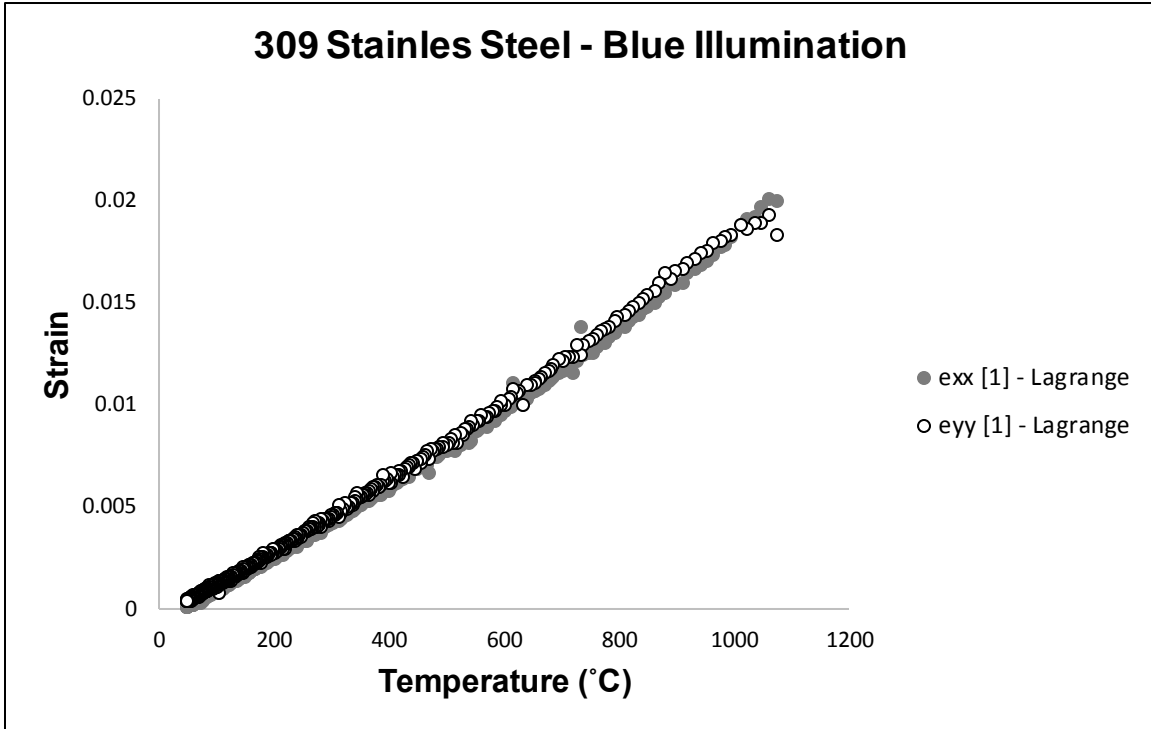
Figure 3.11. Variation of vertical (ε_{yy}) and horizontal (ε_{xx}) strains with respect to temperature for 309 Stainless Steel with blue illumination
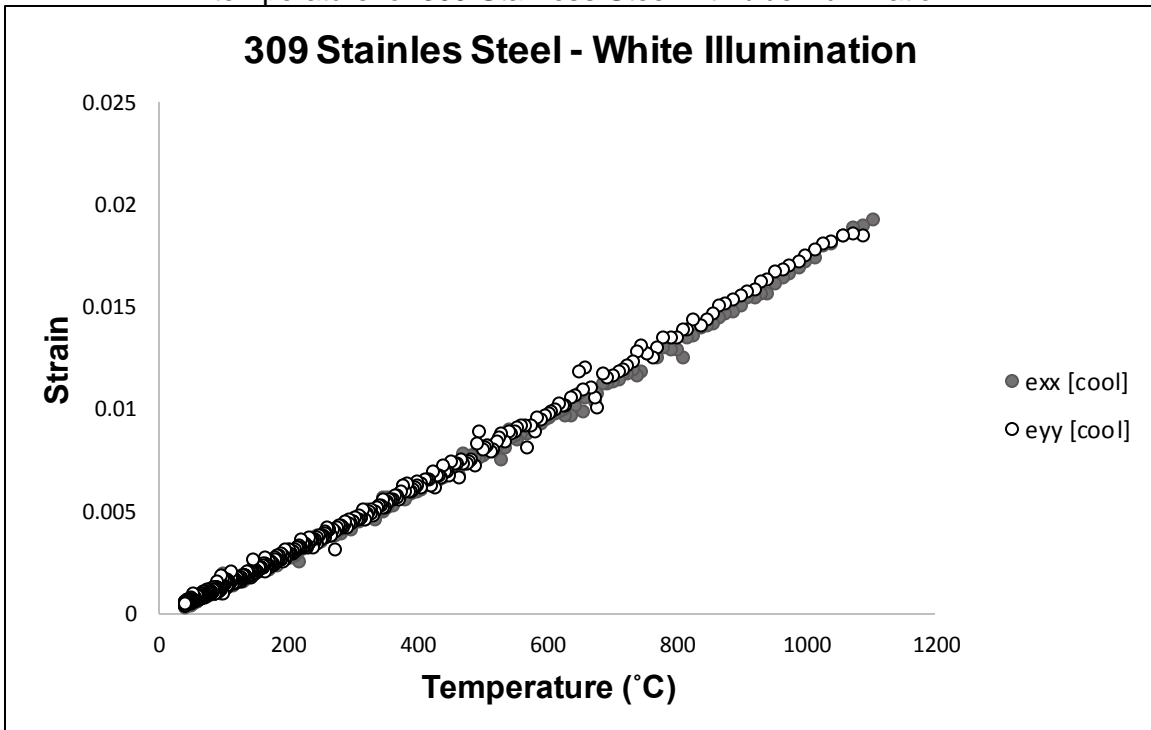
Figure 3.12. Variation of vertical (ε_{yy}) and horizontal (ε_{xx}) strains with respect to temperature for 309 Stainless Steel with white illumination
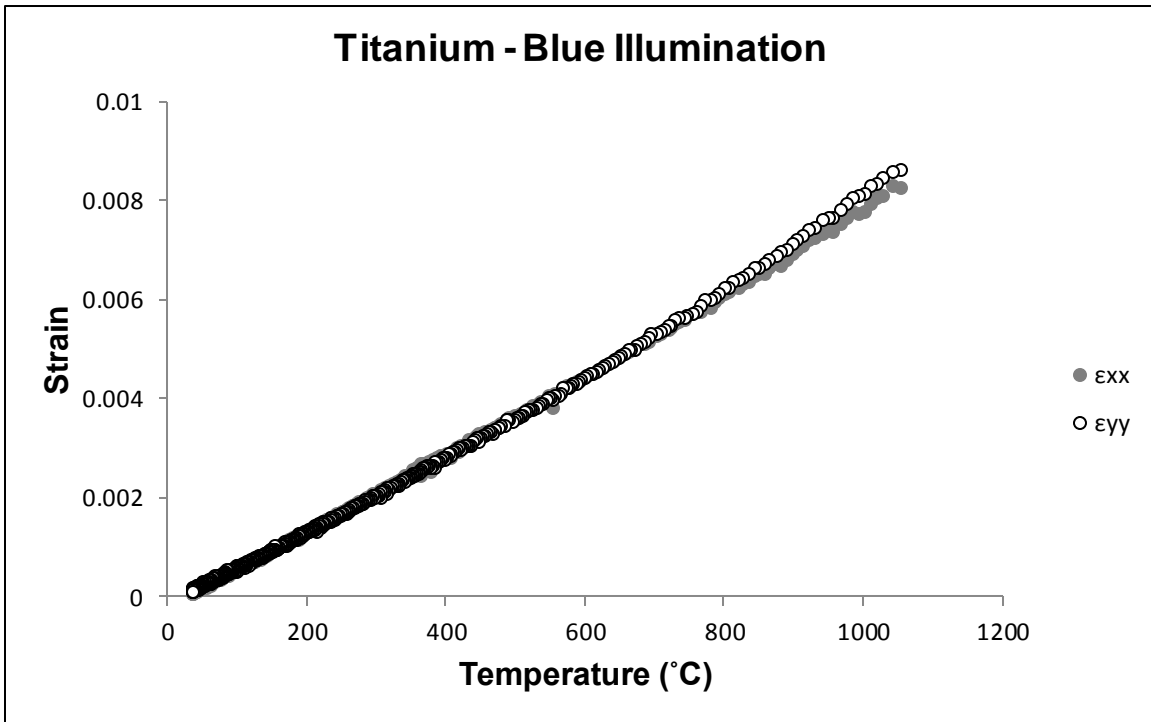
Figure 3.13 Variation of vertical (ε_{yy}) and horizontal (ε_{xx}) strains with respect to temperature for Titanium with blue illumination
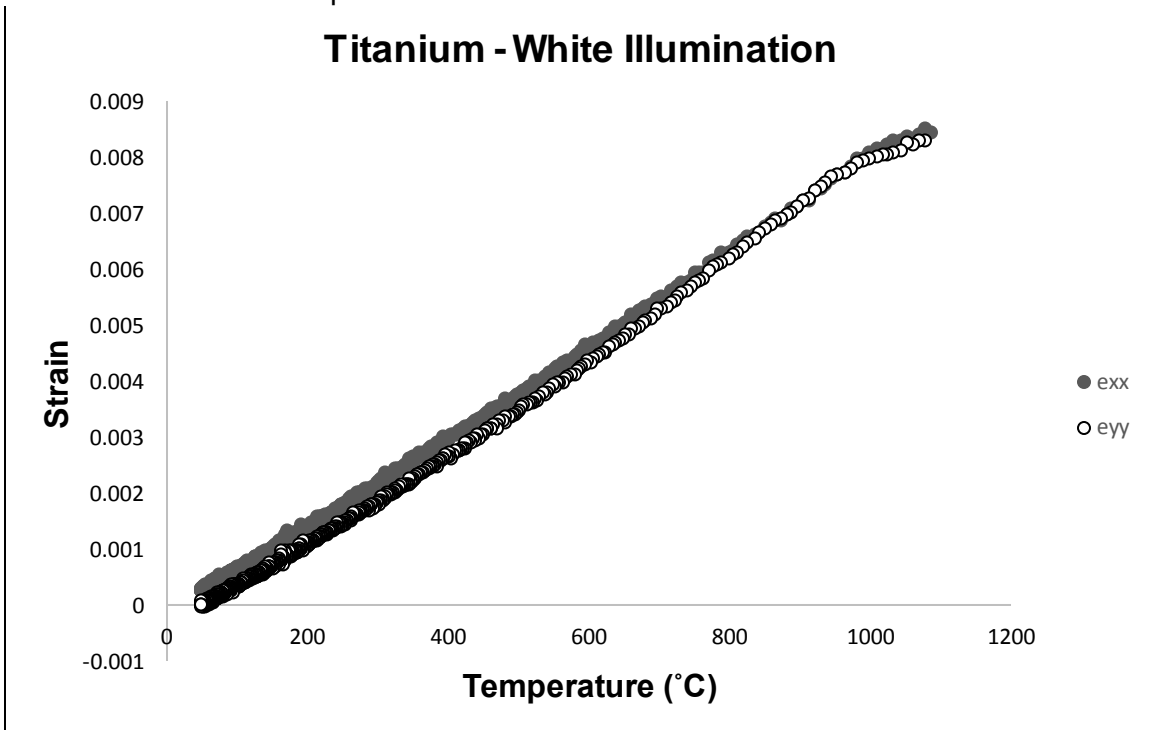
Figure 3.14 Variation of vertical (ε_{yy}) and horizontal (ε_{xx}) strains with respect to temperature for titanium with white illumination

In the previous figures it is observed that both ε_{xx} and ε_{yy} evolve in a very similar way with respect to temperature, this also indicates the isotropic thermal expansion response of both materials.

The coefficient of thermal expansion (α) is calculated by taking the derivative with respect to the temperature:

$$\alpha(T) = \frac{d\varepsilon(T)}{dT} \tag{2}$$

The best quadratic polynomial was fitted to the ε vs. T graphs shown above, and the derivative was calculated to obtain values of α at each temperature. The quadratic fitted ε vs. T curve shown in the next equation was taken from the average horizontal and vertical strain vs temperature curve of the 309 stainless steel specimen using white illumination, Figure 3.12.

$$\varepsilon(T) = 2.565 * 10^{-9}T^2 + 1.481 * 10^{-5}T - 1.704 * 10^{-4} \qquad 30^o C < T < 1100^o C$$

$$\tag{3}$$

After derivation:

$$\alpha(T) = 2 * 2.565 * 10^{-9} * T + 1.481 * 10^{-5} \tag{4}$$

Using the α(T) equation (4), a graph was constructed for each illumination condition and compared with the literature CTE values for both 309 stainless steel

and titanium from North American Stainless Steel and ASM Material Data sheet, respectively.
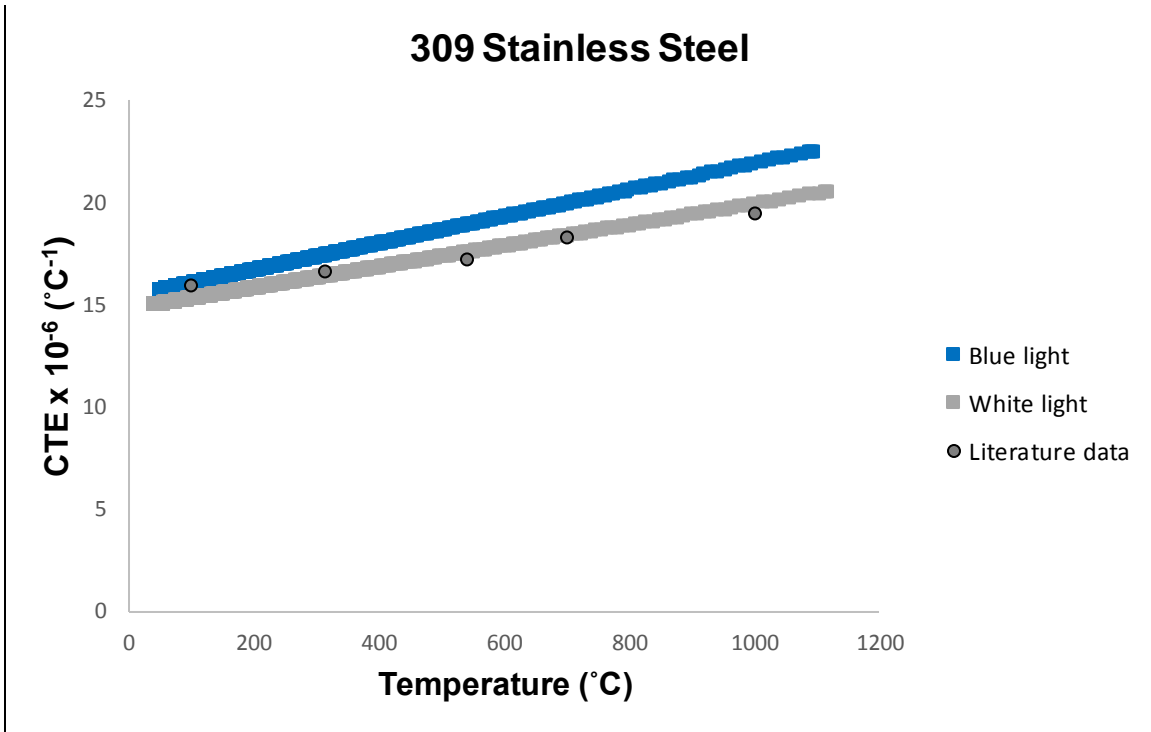
Figure 3.15. Variation of CTE with respect to temperature for 309 stainless steel

Figure 3.15 shows the results in this work compared to the values found in the literature for 309 stainless steel. It is observed that the values obtained in this work are in good agreement with those found in the literature, with a maximum difference of about 4% using white light. This small difference might be due to possible differences in the material's chemical composition, as well as the experimental methodology conducted to measure the CTE in the literature.

The following figure shows the CTE values calculated in this work for both illumination conditions for titanium grade II. A discrepancy is observed for white light versus blue light. However, it is difficult to compare this values with the published ones in the literature, for the reason that there are discrepancies within different sources in the literature for this material. This might be because of differences in the chemical composition of the titanium material. At 100°C the difference with respect to one literature source (www.swissprofile.com) using blue light is 2%, and at 500 °C, the difference is 13 %.
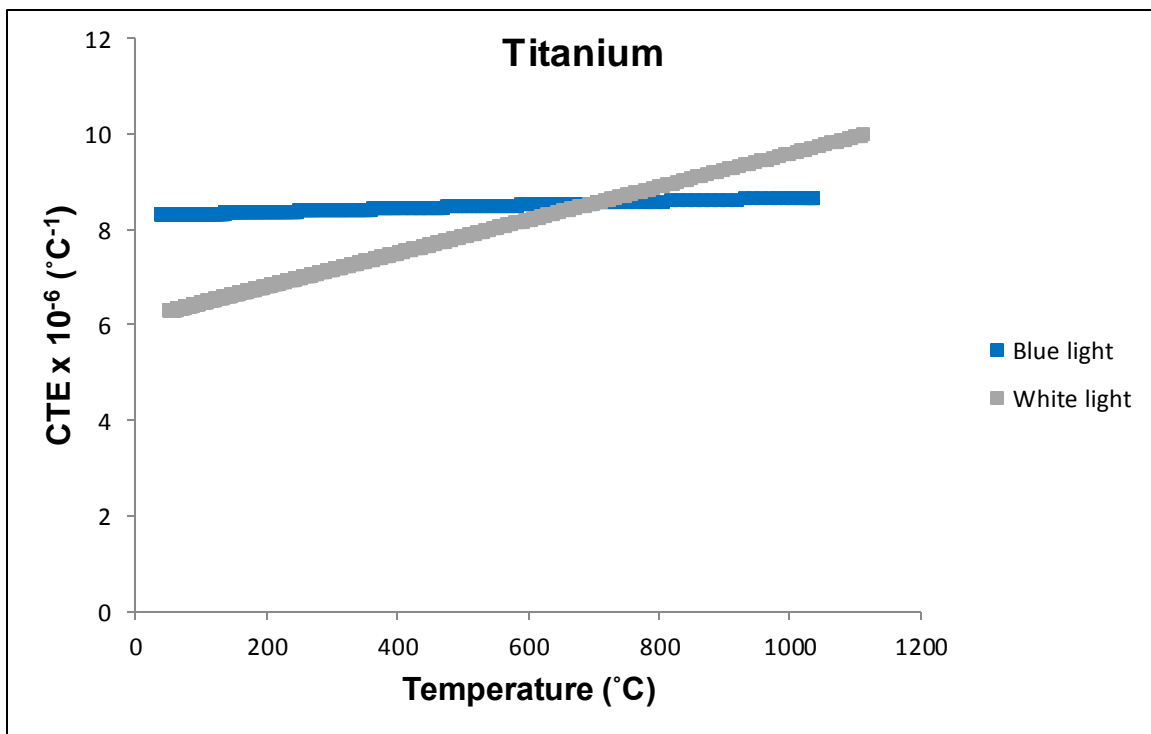
Figure 3.16. Variation of CTE with respect to temperature for titanium grade II

3.4 SUMMARY AND CONCLUSIONS

The proposed 3D DIC experimental approach was successfully applied to different materials at temperatures ranging from room temperature to 1100˚C. The use of a blue band pass optical filter provided high quality images at all temperatures. A standard deviation of < 3% of the micro strain was found between the 10 images taken at each temperature step for all cases (blue light, white light, with fan and no fan), indicating the high level of accuracy in the strain measurements of this technique. No particular trend was observed using white or blue illumination and/or with and without the use of a fan; therefore, heat haze is not a influencing factor for this technique.

In section 3.3 the values of the CTE of two materials: 309 stainless steel and titanium grade II were successfully calculated and compared with the data available in the literature. A maximum difference of 4% was obtained between the measurements in this work and the values reported in the literature for stainless steel using white light illumination. This difference might be due because of differences in the material's chemical composition, as well as the experimental methodology conducted in the literature to measure the CTE of these materials.

It is important to note that the ultra-high temperature resistant Yttrium Oxide white spray paint and the silica-based ceramic black paint, used for the speckle pattern, remained unaffected for numerous high temperature tests proving its successful performance for this application.

CHAPTER 4
HIGH TEMPERATURE TENSILE RESPONSE

4.1 INTRODUCTION

Determining the mechanical response of materials at elevated temperatures is a subject of great interest in metal forming, aerospace and aero-engine industries. Measurement of the deformation response under tensile loading at high temperatures is crucial for establishing thermomechanical and thermophysical properties of materials, consequently, determining the reliability of a component or structure exposed to elevated temperatures. However, there are certain challenges associated with accurate measurement of high temperature tensile response of materials [1, 2]. Conventionally, high temperature tensile behavior of an engineering material is obtained by conducting tests at well-controlled environments, and measuring the deformation response using extensometry. Extensometry here can be referred to either contact or non-contact methods. Although this methodology provides acceptable results and is widely used in engineering applications, accuracy of the deformation measurements will be highly sensitive to the testing equipment. Moreover, in cases where the presence of local phenomena gives rise to considerable localization of deformation, extensometer-based strain measurements may not provide

quantitative evidence on such deformation localization phenomena. On the other hand, recently developed temperature-resistant strain gauges provide a more reliable approach for strain measurements performed at significantly high temperatures, with the capability to measure the strain localizations [3]. However, the application of such temperature-resistant strain gages is limited due to their point measurement capabilities, as well as their maximum working temperature.

Recent advances in the area of non-contact full-field measurements have proven to provide reliable substitutes for the conventional material testing methods. In particular, digital image correlation (DIC) is one of the most appealing techniques with the capability of providing accurate information on the deformation response of materials subjected to extreme conditions, with the benefit of use of straightforward specimen preparation [4]. DIC has the capability to adjust the spatial resolution, ability to take measurements on curved surfaces [5] and different specimen sizes and/or shapes [6 – 8] and also the suitability for static and high speed measurements [9, 5]. There have been studies where high temperature DIC has been used to measure specimen deformation from room temperature up to 2600℃ [10]. The first work in this area was performed by J. S. Lyons et al [1] in 1996. In this study, the authors conducted a series of experiments to assess the capabilities of 2D DIC in the measurement of full-field deformations at elevated temperatures. It was found that the variations in the refractive index of heated air outside the furnace can result in substantial image distortions. It was also found in this work that the visible thermal radiation emitted by the material when heated to temperatures above 650-700ºC alters the contrast and the intensity of the speckle

46

pattern, and consequently introduces significant amounts of errors to the image correlation process. More recent works have studied DIC for measuring strains at temperatures ranging from room temperature to 1200°C. Grant et al [11] presented a method that overcomes the black body radiation issue by implementation of optical filters and special illumination sources, providing accurate DIC measurements up to 1100°C.

Another limitation associated with the application of DIC at high temperatures is due to the deteriorating effect of extreme temperatures on the speckle pattern. In recent years, the application of novel speckling methods capable of sustaining integrity and efficiency at extreme temperatures has been studied. Application of temperature-resistant coatings such as LSI boron nitride and aluminum oxide-based ceramic coatings [1], temperature resistant white Y_2O_3 paint and other ceramic paints [12] a mixture of black cobalt oxide with liquid commercial inorganic adhesive [2] and the use of plasma sprayed tungsten powder as the speckle pattern are examples on novel speckling methods facilitating the application of DIC in temperatures up to 2600°C [10].

With the rapidly growing applications of digital image correlation in the area of material characterization, further research is required to establish simpler high temperature DIC techniques that overcome the previously described limitations. It is also beneficial to devise experimental techniques that employ portable heating systems compatible with multiple testing machine configurations and for different sample size and geometries, in order to take advantage of the convenience of the DIC's simple and versatile setup equipment. In light of this, the present work

47

focuses on the application of a portable novel high temperature 3D DIC measurement system that can be employed with a wide range of specimen geometries and sizes. The effectiveness of the system is verified by successfully conducting tensile experiments at temperatures up to 900°C to study the thermomechanical properties of a 304 stainless steel specimens. The advantage of conducting full-field measurements over the conventional test methodologies are highlighted in an analytical study based on the method of virtual fields, which facilitates the identification of the constitutive response of the material with high accuracy.

4.2 HIGH TEMPERATURE TENSILE TEST

4.2.1 Material and Specimen Geometry

Flat dog-bone specimens were extracted from an as-received plate of commercially available low-carbon 304 stainless steel. This material was selected due to its non-magnetic and superior scaling resistance characteristics. The tensile specimens were coated with a thin layer of ultra-high temperature resistant white paint and a high temperature black silica-based ceramic paint is then applied on top of the white coating to obtain a fine speckle pattern, used for the image correlation purposes. Black speckle particles with an average size of 20 μm are produced in this way. Specimens were kept at room temperature for 24 hours to

let the paint fully dry. Figure 4.1 illustrates a speckled tensile specimen with a magnified view of the speckle pattern in the area of interest.
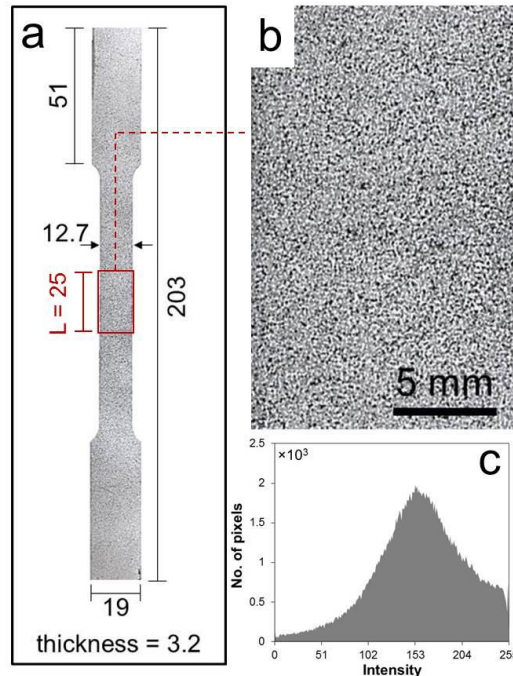
Figure 4.1. (a) Tensile specimen geometry with a magnified view of the area of interest and its corresponding gray scale histogram shown in (c). All dimensions in mm.

4.2.2. Tensile Tests

Tensile tests were first carried out at room temperature to obtain the reference stress-strain response of the material. To do so, the specimen is inserted into the grips of a conventional tensile frame and pulled to tension in displacement control mode at a constant cross-head speed of 10 mm/min. The tensile load is measured by the machine load-cell, and converted to true stress later. True strain and strain rates are determined using the full-field strain data obtained from DIC, as explained in detail later.

To study the high temperature tensile response of the specimens and determine their properties, the same tensile frame is used. To conduct experiments at high temperatures, an induction heating system was used in conjunction with the tensile frame. The induction heating system employed here is a portable table-top unit suitable to heat up a wide variety of specimen geometries and dimensions [13] and can be coupled with various testing machines, as long as it is equipped with an appropriate coil system. The induction heater is equipped with a water-cooled copper coil system that heats up the specimen at a rate of 1.6^{o}C/s and provides relatively uniform temperature distribution in the heated area. Prior to the onset of the tensile experiments, the steel specimen was clamped at the bottom grip of the tensile machine inside the coil and heated up to the target temperature. After a dwelling time of several minutes allowed for the temperature to become uniform, the specimen is clamped at the top grip and the test is immediately initiated. Tensile tests are initiated when the specimen temperature reaches the target temperature. Target temperatures used in this work are 300°C, 500°C, 700°C and 900°C. The temperature of the specimen was measured during the tensile experiments using a non-contact infra-red thermometer, with a nominal measurement accuracy of ±3°C. The temperature history of the specimen at the location of the area of interest was recorded at the same sampling rate used for load and image acquisitions. Reproducibility of the results is ensured by conducting several tests per target temperature. The next figure illustrates the experimental setup in this work.
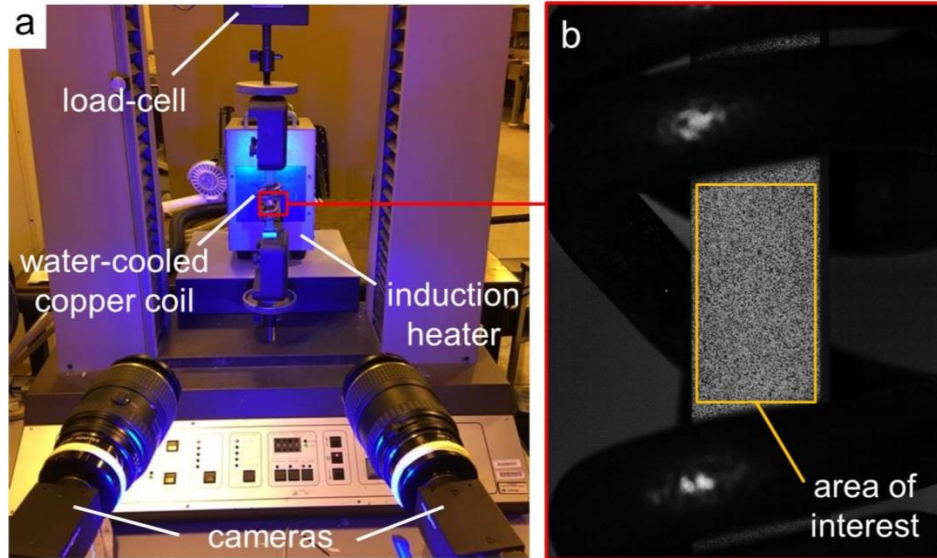
Figure 4.2. (a) Experimental setup with a magnification of the area of interest shown in (b).

4.2.3. Imaging and Digital Image Correlation

3D digital image correlation was utilized to provide information on the full-field deformation response of the specimens subjected to high temperature tension. To this purpose, a pair of 5 MP CCD cameras, each equipped with a 100 mm macro lens is used to acquire stereo images during deformation. Images were captured from the area of interest at full-field resolution of 2448×2048 pixel^2. The stereo images were acquired continuously from a 25×12.7 mm^2 area of interest located at the center of the specimen surface (see Figure 4.2-b), at a rate of 1 frame per second. Image acquisition rate was synchronized with the load-cell data sampling rate via a data acquisition box.

Radiation of a heated object can significantly alter the intensity of the images captured by ordinary imaging equipment, as stated earlier in this work.

Such variation in the intensity of images at high temperatures can introduce significant error to the image correlation process, therefore needs to be compensated. The variation of image intensity is proportional to the spectral energy emitted from a heated object, whereas the radiation energy is itself a function of temperature and wavelength, as described by the Planck's radiation law:

$$I(\lambda,T) = \frac{2hc^2}{\lambda^5} \frac{1}{e^{hc/\lambda kT} - 1} \tag{5}$$

where $I(\lambda,T)$ is the spectral radiation energy, λ is wavelength, T is absolute temperature; h, c and k are Planck's constant, speed of light and the Boltzmann constant, respectively. Variation of spectral energy with respect to temperature is plotted in the next figure for three wavelengths in the range of visible light. It is clearly indicated that the radiation energy increases substantially at temperatures > 700°C, while this increase is more significant at larger wavelengths. It is noted that the energy variation of the wave with the shortest wavelength is negligible compared with the other two waves. The shortest wavelength shown here (450 nm) corresponds to the visible blue light, indicating that the use of blue light illumination can considerably reduce the error due to the intensity change.
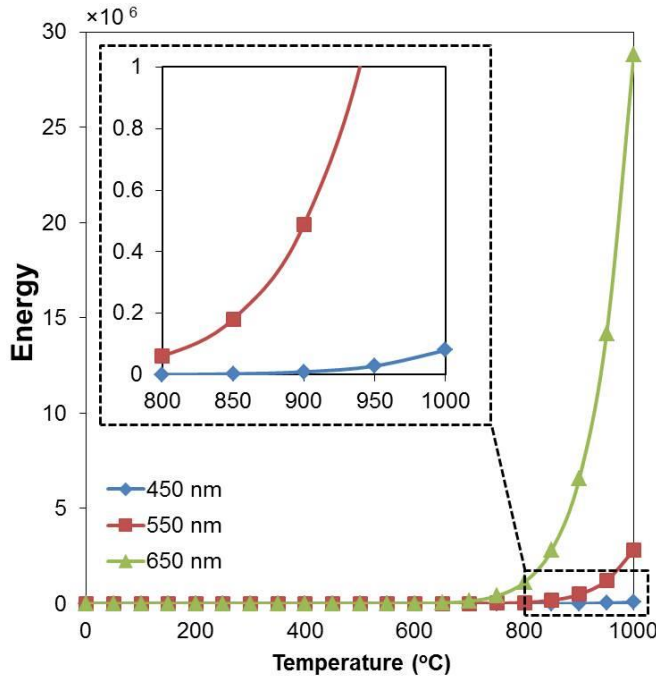
Figure 4.3. Variation of radiation energy with temperature, for three different wavelengths within the range of visible light.

In addition to the light source, the imaging system must also be equipped with appropriate filters which allow for the transmission of a specific range of wavelengths consistent with that of the illumination source. Accordingly, blue band pass filters (BP470, supplied by Midwest Optical Systems, Inc.) with a wavelength range of 425-495 nm were used to eliminate the contribution of unwanted wavelengths. The other beneficial effect of blue band pass filters is due to the consistence of their transmission efficiency with the quantum efficiency of the utilized camera system. As depicted in Figure 4.4, the maximum transmission efficiency of the blue band pass filters takes place in a range of wavelengths over which the quantum efficiency of the camera is also highest.
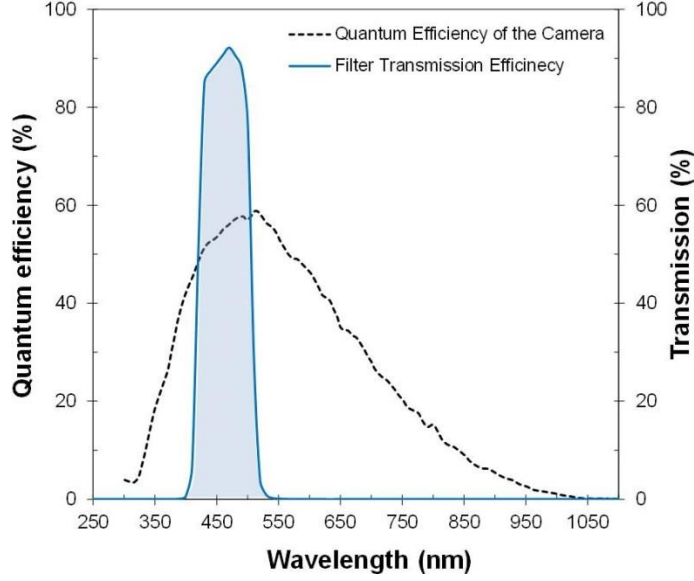
Figure 4.4. Variation of quantum efficiency of the camera and the transmission efficiency of the utilized band-pass filter as a function of wavelength.

Images captured during specimen deformation were used as the input to the software Vic-3D for image correlation and further quantitative analysis. Details concerning the image correlation process are reported in the following table. Different strain components were computed using the full-field displacement data employing a Gaussian filtering and the filter size of 15. The strain rate is calculated over the area of interest using the full-field strain data and applying a simple central difference scheme as:

$$\dot{\varepsilon}_{yy}(t) = \frac{\varepsilon_{yy}(t + \Delta t) - \varepsilon_{yy}(t - \Delta t)}{2\Delta t} \tag{6}$$

where subscript 'yy' denotes vertical direction, and Δt is interframe time ($\Delta t = 2$ s).

Table 4.1. Image correlation details used in the present study

Full-field measurement technique		3D DIC (Vic-3D)
Subset		25×25 pixel^2
Step		6 pixel
Magnification factor		20 μm/pixel
Strain filtering (filter size)		Gaussian (15)
Matching criterion		Normalized squared
Interpolation		Optimized 8-tap interpolation
Shape function		Affine
Strain resolution:	350˚C	110 με
	600 ˚C	324 με
	800 ˚C	360 με
	900 ˚C	400 με

4.3 IDENTIFICATION OF VISCO-PLASTIC CONSTITUTIVE RESPONSE

The objective in this work is to utilize the virtual fields method (VFM) in conjunction with our full-field measurements to identify the visco-plastic constitutive response of the examined material over a temperature range of 25°C to 900°C. To this purpose, the constitutive response of the material is first considered to take the general form of the Johnson-Cook model [14] as:

$$\bar{\sigma} = \left(A + B\bar{\varepsilon}_p^n\right)\left(1 + C\ln\dot{\varepsilon}^*\right)\left(1 - T^{*m}\right) \qquad (7)$$

where $\bar{\sigma}$ and $\bar{\varepsilon}_p$ are flow stress and effective plastic strains, respectively. $\dot{\varepsilon}^*$ denotes plastic strain rate normalized with the reference quasi-static strain rate, and T^* is the homologous temperature, defined as:

$$T^* = \frac{T - T_0}{T_M - T_0} \qquad\qquad (8)$$

in which T_0 and T_M represent reference temperature (298 K) and absolute melting temperature (1700 K) of the material. Parameters A, B, n, C and m in Eq. 7 are key material constants that need to be identified experimentally. The first three constants, i.e. A, B and n can be readily obtained from the quasi-static stress-strain curve extracted at reference strain rate and temperature conditions and by the use of simple curve fitting. Figure 4.5 shows the experimental flow curve plotted at reference strain rate and temperature. Accordingly, parameters A, B and n are identified as 393 MPa, 743.1 MPa and 0.568, respectively, at a reference strain rate of 4.7×10^{-4} s^{-1}.
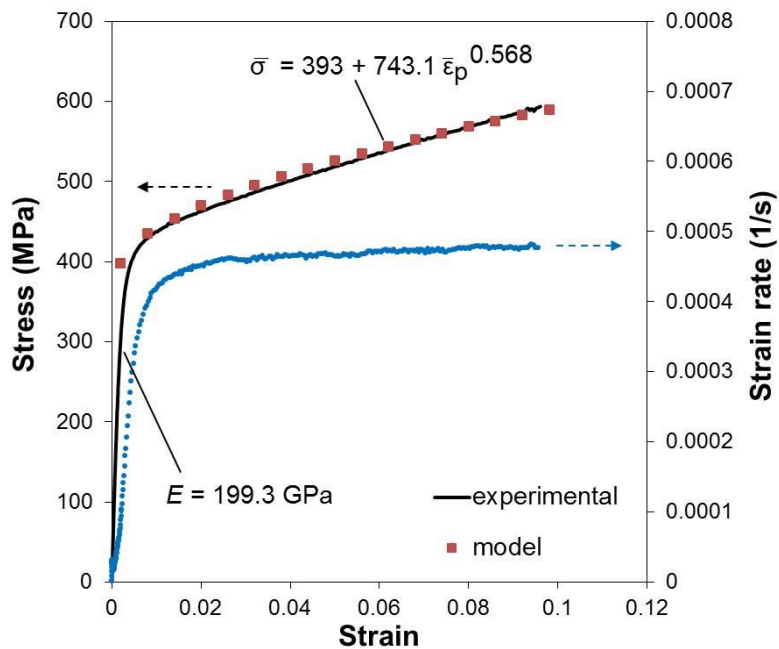
Figure 4.5. Experimental and model curves obtained at reference temperature (T_0 =298 K) and reference strain rate 4.7×10^{-4} s^{-1}.

The main idea here is to identify the other material parameters C and m using the method of virtual fields. In quasi-static deformation, the principle of virtual work can be written as:

$$-\int_V \sigma_{ij} \varepsilon_{ij}^* dV + \int_{S_V} T_i u_i^* dS + \int_V f_i u_i^* dV = 0 \qquad (i, j) = (1,2,3) \qquad (9)$$

where σ_{ij} and T_i denote the components of stress tensor and traction vector, respectively. f_i is the volumetric force vector. V is the volume over which the equilibrium is written, and S_V represents the boundary surface of V. u_i^* denotes the components of a "virtual displacement field" and ε_{ij}^* are the components of the virtual strain tensor derived from u_i^*. In comparison with the magnitude of the tensile load applied on the specimen, volume forces are neglected in this work. Eq. 7 remains valid for any specimen in quasi-static equilibrium as long as a kinematically admissible virtual displacement field is incorporated. For the specific case of uniaxial tension, the virtual displacement field suggested by Avril et al. [15] is adopted in this work. Accordingly, the virtual displacement and strain components are expressed as:

$$\begin{cases} u_x^* = 0 \\ u_y^* = y \end{cases} \qquad \begin{cases} \varepsilon_{xx}^* = 0 \\ \varepsilon_{yy}^* = 1 \\ \varepsilon_{xy}^* = 0 \end{cases} \qquad (10)$$

The virtual field described in Eq. 10 is defined over the area of interest used in full-field measurements, shown schematically in Figure 4.6.
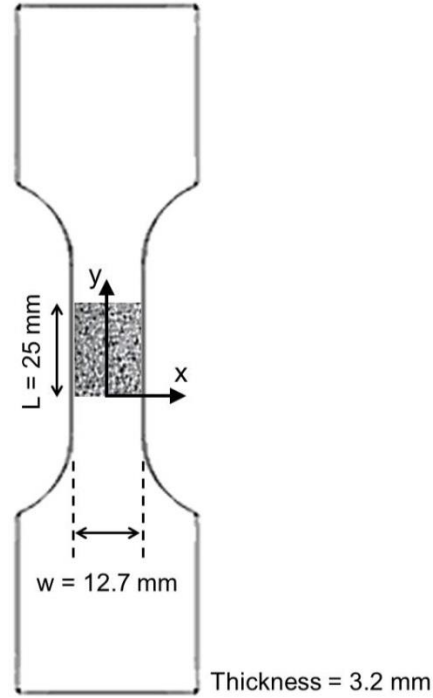
Figure 4.6. Schematic of the tensile specimen with the dimensions of the area of interest on which full-field measurements are conducted.

Assuming that the surface measurements remain valid through the thickness of the specimen, after substituting the virtual displacement and strain fields in Eq. 3 the equilibrium equation can be rewritten in the simple form:

$$-t\left[\int_S \sigma_{yy}(\tau)dS\right] + P(\tau).L = 0 \tag{11}$$

where P is the measured far-field tensile load; t and L represent thickness and length of the area of interest, respectively. S is the area on which full-field measurements are performed, and τ is time. In case of uniaxial tension, the equivalent stress $\bar{\sigma}$ is equivalent to the vertical component of the stress tensor σ_{yy}. Therefore, Eq. 11 can be further simplified as:

58

$$\int_S \overline{\sigma}\left(\overline{\varepsilon}_p, \dot{\varepsilon}^*, T^*, C, m, \tau\right) dS = \frac{P(\tau).L}{t} \tag{12}$$

Note that the constants *A*, *B* and *n* are already identified at this point. Thus, the only unknown parameters in Eq.12 are material constants *C* and *m*. Due to the presence of experimental noise in the load and full-field deformation measurements, the unknowns in Eq. 12 may not be directly evaluated. Instead, to determine the constants *C* and *m* an iterative solution algorithm is implemented in which a cost function, Φ, is minimized with respect to the unknown parameters:

$$\Phi(C,m) = \sum_{i=1}^{N} \sum_{\tau=\tau_0}^{\tau=\tau_f} \left(\frac{1}{S} \int_S \overline{\sigma}\left(\overline{\varepsilon}_p, \dot{\varepsilon}^*, T^*, C, m, \tau\right) dS - \frac{P(\tau).L}{St} \right)^2 \tag{13}$$

Eq. 9 defines the cost function Φ as the quadratic deviation between the average flow stress measured from the average plastic strain, strain rate and temperature within the area of interest and the stress measured from the far-field tensile load, summed up over the duration of the experiment. τ_0 and τ_f in Eq. 13 denote the instants of the plastic deformation initiation (yielding) and plastic instability (necking), respectively. *N* denotes the total number of experiments conducted at different temperatures ranging from room temperature to 900°C, and at various strain rates. The advantage of the application of such cost function over the traditional finite element model updating (FEMU) is explained in [15].

Note that the integral term in Eq. 13 can be approximated as the average flow stress of the material at area *S*. To evaluate average $\overline{\sigma}$ in *S*, spatial averaging

of $\bar{\varepsilon}_p$, $\dot{\varepsilon}^*$ and T^* can be conducted within area S, and the integral term can be simplified as:

$$\int_S \bar{\sigma}\left(\bar{\varepsilon}_p, \dot{\varepsilon}^*, T^*, C, m, \tau\right) dS \approx \bar{\sigma}\left(\underline{\bar{\varepsilon}}_p, \underline{\dot{\varepsilon}}^*, \underline{T}^*, C, m, \tau\right) w.L \qquad (13)$$

where underline denotes the spatially averaged value over the entire area of interest. Spatial averaging in this case is possible only on condition that the spatial variabilities of strain, strain rate and temperature in the area of interest are negligible. In cases where a considerable variability in any off the variables is present, the procedure detailed in [15, 16] can be adopted. Figure 4.7 depicts typical strain maps extracted at different strain magnitudes for a tensile test initiated at 900°C. Relatively uniform distribution of axial and lateral strain components in the area of interest is clearly evidenced, confirming the possibility to conduct spatial averaging of strain (and strain rate) in this work.
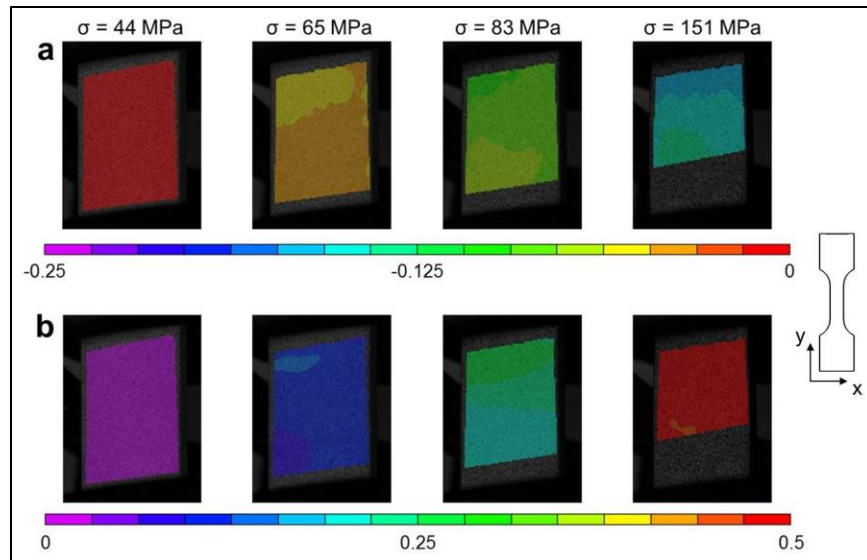
Figure 4.7. Strain maps showing the distribution of (a) ε_{xx} and (b) ε_{yy} over the area of interest at different stress magnitudes ($T = 900$°C).

4.4 RESULTS AND DISCUSSIONS

Occurrence of localized deformation can result in a significant deviation between the stress-strain curves extracted using conventional extensometry and full-field measurements. There is considerable deformation localization in tensile experiments conducted in this work, which is due to the local heating of specimens within their gage area. Figure 4.8 shows photographs of an undeformed and a fractured specimen.

The fractured specimen indicates considerable localized deformation, resulted from the formation of a necked area at the heated zone of the specimen. The application of DIC in this case facilitates the averaging of strain data over an area of interest which encompasses the localized necking zone, thus giving a more accurate measure on the extent of deformation applied on the specimen. On the other hand, strain measurement based on cross head displacement significantly underestimates the strain applied on the specimen by smearing out the effect of locally-developed strains. This is shown in Figure 4.9, where a comparison has been made between the stress-strain curves plotted using the cross-head displacement and DIC measurements.

Figure 4.8. Photograph of (a) undeformed and (b) fracture specimen tested at 900°C. Location of the necking zone has been magnified in (c).

Figure 4.9. Engineering stress-strain curves obtained using cross-head displacement and DIC (T = 900°C)

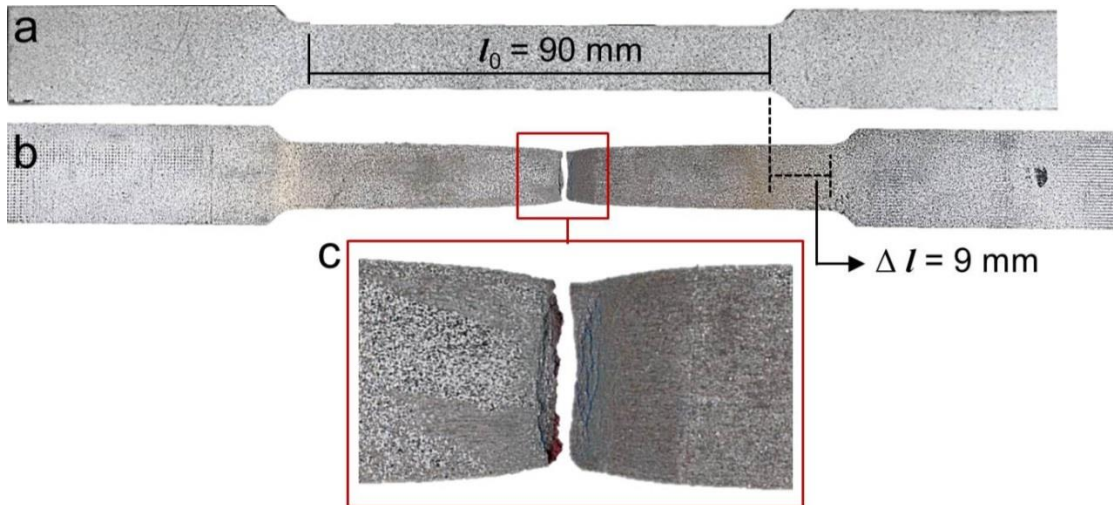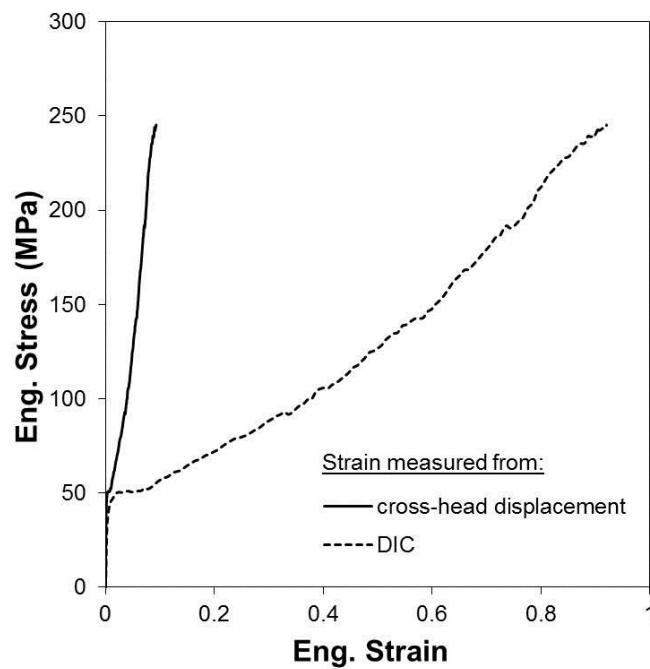Next, to determine the Johnson-Cook parameters C and m, experimental stress-strain curves are considered. The 0.2% offset method is used to obtain the plastic portion of the curves. Figure 4.10 illustrates true stress-strain curves plotted in plastic region along with their corresponding temperature history curves. It is clearly seen that temperature of the specimen at the location of the area of interest undergoes a constant decrease during the experiment. This might be due to the fact that as the specimen is pulled in the axial direction, its cross sectional area is constantly reduced due the Poisson's effect, increasing the distance between the specimen surface and the heating coil; consequently, the efficiency of induction heating is continuously decreased. Continuous temperature decrease occurred during the experiment can be superimposed to the strain hardening response of the material to result in a progressive hardening of the specimens over the duration of the experiment. In addition although the same cross head speed was used in all experiments, local strain rate was also found to have varied during each experiment. Evolution of strain rate is shown in Figure 4.11, indicating variations of up to two orders of magnitude in the strain rate values applied to different specimens in this work. The reason for the trends observed in Figure 4.11 is not fully understood here, but it can be attributed to the complex deformation mechanisms due to the constant variation of temperature during tensile experiments in this work. It is beyond the objective of this wok to elucidate the unusual trends observed in the strain rate and temperature observed here. However, the constant variations observed in both temperature and strain rate history curves can be turned into advantage, since they allow for the identification

of a single thermo-visco-plastic constitutive law over a wide range of temperature and strain rates, using a minimum number of tests. In this regard, the key Johnson-Cook parameters *C* and *m* can actually be identified taking into account the entire population of data points obtained in this work. Once the material parameters *C* and *m* are identified, experimental stress-strain curves can be corrected and replotted at constant temperature and strain rate conditions.

In the present work, the following approach is proposed to identify the material constants *C* and *m*:

1. Collect the entire population of data points obtained from tensile experiments. Each data point within this collection contains a unique set of load, strain, strain rate and temperature information obtained at a given time.

2. Select an initial guess for the unknown Johnson-Cook parameters *C* and *m*. Calculate the flow stress, $\bar{\sigma}$, using the guessed values of *C* and *m*, along with the strain, strain rate and temperature values collected in step 1. Note that other model parameters *A*, *B* and *n* are already known at this point and can be directly substituted in Eq. 7 to calculate $\bar{\sigma}$. The initial values of *C* = 0 and *m* = 0 are considered as the starting point in this work.

3. Evaluate the cost function Φ (Eq. 13) using the computed $\bar{\sigma}$ and the measured far-field tensile load *P*.

4. Update *C* and *m*, and repeat steps 2 and 3 for the updated values of these constants. In order to ensure the uniqueness of the results, minimization of the cost function Φ must be carried out over a wide range of values for *C*

64

and *m*. In the present work, updating the temperature parameter *m* is conducted by constantly increasing *m* from *m* = 0 to *m* = 1 at increments of 0.02. Similarly, *C* is updated over a range of 0 to 0.4 in increments of 0.05.

5. Identify the pair of *C* and *m* values that minimizes the cost function.

Figure 4.12 depicts the variation of cost function with the unknown model parameters *C* and *m*. Theoretically, Φ must be zero when actual material parameters are implemented. However, due to the presence of measurement noise and the approximation of the real material response by an empirical model, i.e. Johnson-Cook model here, achieving a zero value for Φ is not practically possible. As shown in Figure 4.12, the cost function is well-conditioned and shows a unique minimum for a set of *C* = 0.18 and *m* = 0.36. Accordingly, the final Johnson-Cook model parameters for the examined 304 stainless steel are listed in Table 4.2.

Experimental stress-strain curves shown earlier in Figure 4.10 can now be corrected and replotted at constant temperature and strain rates. Figure 4.13 illustrates a comparison between the experimentally obtained and corrected stress-strain curves. The difference between the two curves is more significant at higher plastic strains. In addition, the maximum relative difference is observed for the case of the specimen tested at 900ºC. This is due to the more substantial variations of strain rate and temperature (see Figure 4.10 and Figure 4.11) occurred during tensile testing of this specimen. It is also clearly seen in Figure 4.13 that the slope of the corrected curves is smaller compared with that of the

uncorrected curves in all temperatures above 20°C. This observation is consistent with the previous statements concerning the higher rate of work hardening in cases where a constant decrease in temperature and/or a continuous increase of strain rate takes place during high temperature tensile tests.

As shown in Figure 4.13, the overall slope of the stress-strain curves decreases at higher temperatures, indicating a lower rate of work hardening.
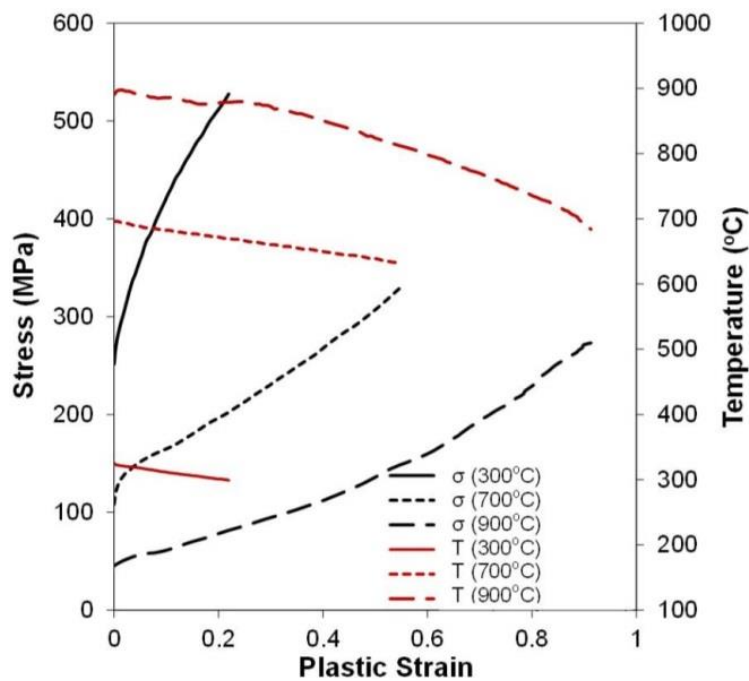
Figure 4.10. Experimental stress-strain curves obtained at varying temperatures.
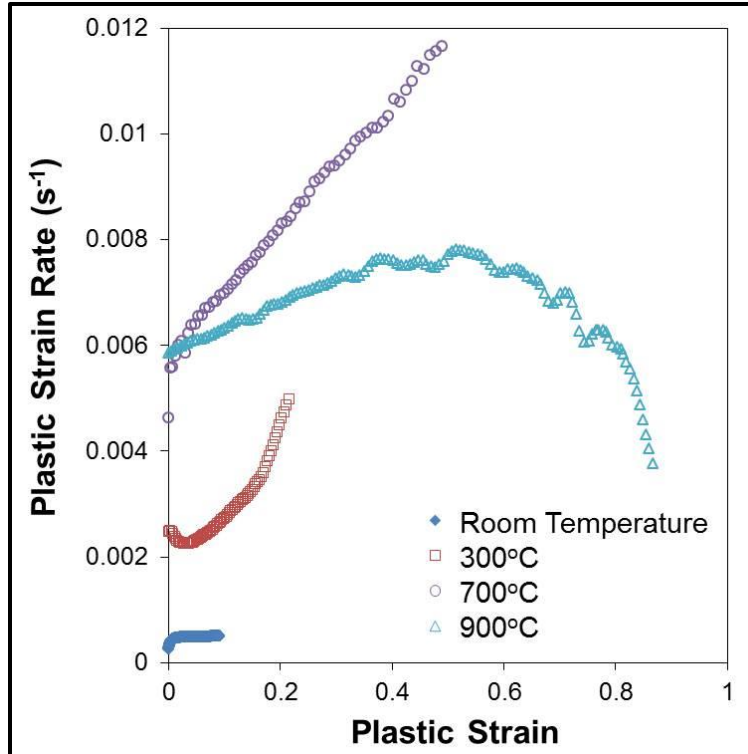
Figure 4.11. Strain rate history curves.
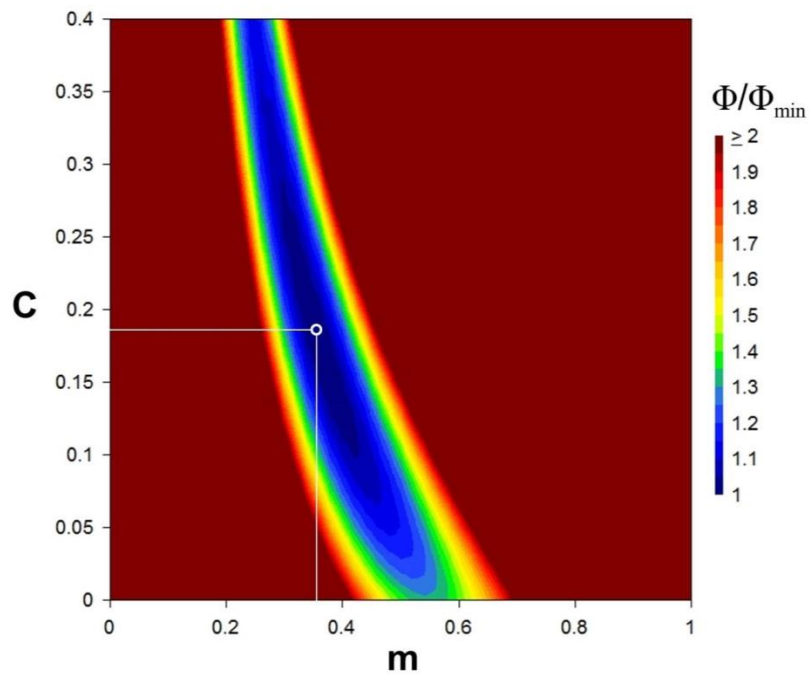
Figure 4.12. Illustration of the value of the cost function normalized by Φ_{min} .

Table 4.2. Johnson-Cook model parameters obtained for the low carbon stainless steel material

A (MPa)	B (MPa)	n	C *	m **
393	743.1	0.568	0.18	0.36

* strain rates range: 4.7×10^{-4} - 1.2×10^{-2}
** Temperature range: $20^{\circ}C$ - $900^{\circ}C$
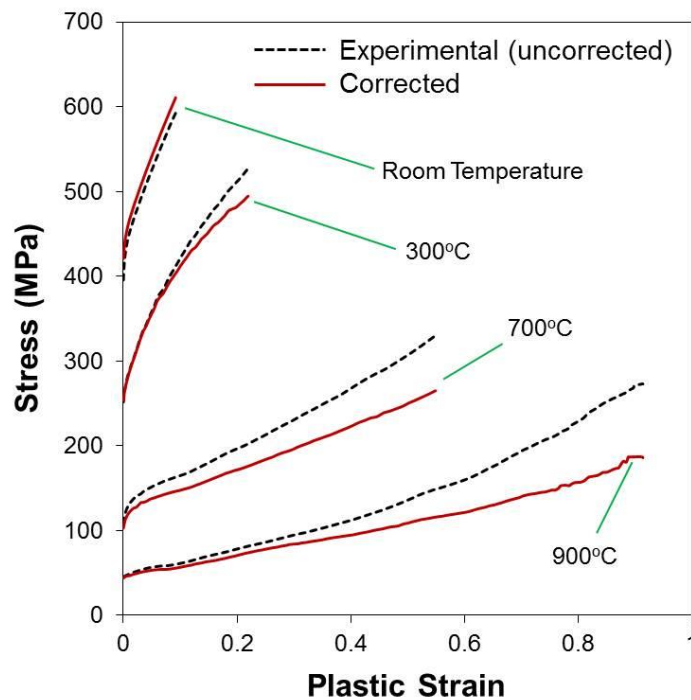
Figure 4.13. Experimental and corrected stress-strain curves. Corrected curves are plotted at constant temperature and constant strain rate of 10^{-3} s^{-1}.

4.5 SUMMARY AND CONCLUSIONS

A series of tensile tests were performed on a 304 stainless steel material exposed to temperatures from $25^{\circ}C$ to $900^{\circ}C$ using the same set up and 3D-DIC

methodology studied in Chapter 3. The full-field strain measurement results were used in conjunction with the VFM to identify the visco-plastic constitutive response of the examined material over this range of temperature. For this, the general form of the Johnson-Cook model was considered for the constitutive response of the material, and the key model parameters were identified using the results obtained from our experiments.

The temperature of the specimen, at the area of interest, experienced a constant decrease as the specimen was pulled in the axial direction. This is possibly due to the progressive decrease in cross sectional area due to Poisson's effect, increasing the distance between the specimen surface and the heating coil around it. The local strain rate was also found to have varied during each experiment. This study took advantage of the temporal variation of strain rate and temperature during deformation time, by identifying a single thermo-visco-plastic constitutive law over a wide range of temperature and strain rates, using a minimum number of tests.

The experimental stress-strain curves obtained from the DIC were successfully corrected for constant temperature and strain rates. The difference between the two sets of curves, i.e. experimentally obtained and corrected curves, was shown to be more significant at higher temperatures.

LIST OF REFERENCES

[1] J. S. Lyons, J. Liu, and M. A. Sutton, 1996, "High-temperature Deformation Measurements Using Digital-image Correlation," Experimental Mechanics, **36**(1), pp. 64-70.

[2] B. Pan, D. Wu, Z. Wang, and Y. Xia, 2011, "High-Temperature Digital Image Correlation Method for Full-Field Deformation Measurement at 1200° C," Measurement Science and Technology, 22, pp. 015701-1-11.

[3] Hitec Products INC, n.d., from http://www.hitecprod.com

[4] M A. Sutton, J J. Orteu and H W. Schreier, 2009, *Image Correlation for Shape, Motion and Deformation Measurements*, Springer. New York, NY.

[5] B. Koohbor, A. Kidane, W. Lu and M.A. Sutton, 2016, "Investigation of the Dynamic Stress–Strain Response of Compressible Polymeric Foam Using a Non-Parametric Analysis," International Journal of Impact Engineering, **91**, pp. 170–182.

[6] B. Koohbor, S. Ravindran and A. Kidane, 2015, "Meso-Scale Strain Localization and Failure Response of an Orthotropic Woven Glass-Fiber Reinforced Composite," Composites Part B: Engineering, **78**, pp. 308–318.

[7] M.A. Sutton, N. Li, D.C. Joy, A. P. Reynolds and X. Li, 2007, "Scanning Electron Microscopy for Quantitative Small and Large Deformation Measurements Part I: SEM Imaging at Magnifications from 200 to 10,000," Experimental Mechanics, **47**(6), pp. 775-787.

[8] R. Ghorbani, F. Matta and M.A. Sutton, 2015, "Full-Field Deformation Measurement and Crack Mapping on Confined Masonry Walls Using Digital Image Correlation," Experimental Mechanics, **55**(1), pp. 227-243.

[9] F. Pierron, M.A. Sutton and V. Tiwari, 2011, "Ultra High Speed DIC and Virtual Fields Method Analysis of a Three Point Bending Impact Test on an Aluminum Bar," Experimental Mechanics, **51**(4), pp. 537-563.

[10] X. Guo, J. Liang, Z. Tang, B. Cao, and M. Yu, 2014, "High-Temperature Digital Image Correlation Method for Full-Field Deformation Measurement Captured with Filters at 2600°C using Spraying to Form Speckle Patterns," Optical engineering, **53**(6), pp. 063101-1-12.

[11] B. Grant, H. Stone, P Withers, and M. Preuss, 2009, "High-Temperature Strain Field Measurement using Digital Image Correlation," Journal of strain analysis for engineering design, **44**(4), pp. 263-271.

[12] B. Koohbor, G. Valeri, A. Kidane, M. Sutton, 2015, "Thermo-Mechanical Properties of Metals at Elevated Temperatures," Advancement of Optical Methods in Experimental Mechanics, **3**, pp. 117-123.

[13] Across International, n.d., from http://www.acrossinternational.com

[14] Frontán J, Zhang Y, Dao M, Lu J, Gálvez F and Jérusalem A, 2012, "Ballistic Performance of Nanocrystalline and Nanotwinned Ultrafine Crystal Steel," Acta Mater, **60**, pp. 1353-1367.

[15] Avril S, Pierron F, Sutton MA and Yan J, 2008, "Identification of Elasto-Visco-Plastic Parameters and Characterization of Lüders Behavior using Digital Image Correlation and the Virtual Fields Method," Mech Mater, **40** pp. 729-742.

[16] Le Louëdec G, Pierron F, Sutton MA and Reynolds AP, 2013, "Identification of the local elasto-plastic behavior of FSW welds using the virtual fields method", Experimental Mechanics, **53** pp. 849-859.

CHAPTER 5
SUMARY AND RECOMMENDATIONS

5.1 SUMMARY

A portable and easy-to-implement experimental method based on 3D-DIC was implemented, and its effectiveness was demonstrated by determining the thermo-mechanical and thermo-physical properties of various materials used in high temperature applications. Sensitivity analyses were performed to study the accuracy of full-field strain measurements on stainless steel and titanium samples in temperatures ranging from RT to 1100°C. Certain challenges associated with the application of high temperature DIC documented in the literature were also studied and overcome. The system was also implemented along with a tensile testing machine to study high temperature tensile response of stainless steel specimen. An analytical approach based on the method of Virtual Fields was implemented to identify the constitutive parameters governing the plastic deformation of the material at high temperatures. The proposed DIC-based technique proved to be a significantly accurate methodology for different specimen geometries and for temperatures ranging up to 1100°C.

5.2 RECOMMENDATIONS

Based on the experience during the experimental studies described in this work, the following recommendations regarding future work efforts in high temperature DIC measurements are presented:

- When performing DIC measurements for temperatures greater than 650°C, the use of a blue bandpass optical filter is required along with a proper white illumination source. Blue LED illumination is not needed.

- For a more accurate thermo-mechanical analysis, it is recommended for future work to employ a full-field temperature measurement equipment such as an infrared camera.

- Other topics of interest in aerospace and military applications for which this technique is suitable are: high temperature DIC with dynamic loading (high strain rate) and high temperature DIC in freely vibrating plates.

REFERENCES

Across International, n.d., from http://www.acrossinternational.com

Aerospace Metals, n.d., from http://www.aerospacemetals.com

AK Steel, n.d., from http://www.aksteel.com

Avril S, Pierron F, Sutton MA and Yan J, 2008, "Identification of Elasto-Visco-Plastic Parameters and Characterization of Lüders Behavior using Digital Image Correlation and the Virtual Fields Method," Mech Mater, **40** pp. 729-742.

B. Grant, H. Stone, P Withers, and M. Preuss, 2009, "High-Temperature Strain Field Measurement using Digital Image Correlation," Journal of strain analysis for engineering design, **44**(4), pp. 263-271.

B. Koohbor, A. Kidane, W. Lu and M.A. Sutton, 2016, "Investigation of the Dynamic Stress–Strain Response of Compressible Polymeric Foam Using a Non-Parametric Analysis," International Journal of Impact Engineering, **91**, pp. 170–182.

B. Koohbor, G. Valeri, A. Kidane, M. Sutton, 2015, "Thermo-Mechanical Properties of Metals at Elevated Temperatures," Advancement of Optical Methods in Experimental Mechanics, **3**, pp. 117-123.

B. Koohbor, S. Mallon, A. Kidane and M. A. Sutton, 2014, "A DIC-Based Study of In-Plane Mechanical Response and Fracture of Orthotropic Carbon Fiber Reinforced Composite," Composites Part B: Engineering, **66**, pp. 388–399.

B. Koohbor, S. Ravindran and A. Kidane, 2015, "Meso-Scale Strain Localization and Failure Response of an Orthotropic Woven Glass-Fiber Reinforced Composite," Composites Part B: Engineering, **78**, pp. 308–318.

B. Pan, D. Wu, Z. Wang, and Y. Xia, 2011, "High-Temperature Digital Image Correlation Method for Full-Field Deformation Measurement at 1200° C," Measurement Science and Technology, 22, pp. 015701-1-11.

Bing P, Kemao Q, Huimin X and Anand A, 2009, "Two-Dimensional Digital Image Correlation for In-Plane Displacement and Strain Measurement: a Review," Measurement Science and Technology, **20**(6), pp. 062001-1-17.

Correlated Solutions, n.d., from http://www.correlatedsolutions.com

D. Zhang and D.D. Arola, 2004, "Applications of Digital Image Correlation to Biological Tissues," Journal of Biomedical and Optics, **9**(4), pp. 691-699.

F. Pierron, M.A. Sutton and V. Tiwari, 2011, "Ultra High Speed DIC and Virtual Fields Method Analysis of a Three Point Bending Impact Test on an Aluminum Bar," Experimental Mechanics, **51**(4), pp. 537-563.

Frontán J, Zhang Y, Dao M, Lu J, Gálvez F and Jérusalem A, 2012, "Ballistic Performance of Nanocrystalline and Nanotwinned Ultrafine Crystal Steel," Acta Mater, **60**, pp. 1353-1367.

H. Su, X. Fang, Z Qu, C. Zhang, B. Yan, and X. Feng, 2015, "Synchronous Full-Field Measurement of Temperature and Deformation of C/SiC Composite Subjected to Flame Heating at High Temperature," Experimental mechanics, DOI 10.1007/s11340-015-0066-5.

J. S. Lyons, J. Liu, and M. A. Sutton, 1996, "High-temperature Deformation Measurements Using Digital-image Correlation," Experimental Mechanics, **36**(1), pp. 64-70.

K. D. Hinsch and H. Hinrichs, 1996, "Three-dimensional Particle Image Velocimetry," Three-Dimensional Velocity and Vorticity Measuring and Image Analysis Techniques, **4,** pp. 129-152.

Le Louëdec G, Pierron F, Sutton MA and Reynolds AP, 2013, "Identification of the local elasto-plastic behavior of FSW welds using the virtual fields method", Experimental Mechanics, **53** pp. 849-859

M A. Sutton, J J. Orteu and H W. Schreier, 2009, *Image Correlation for Shape, Motion and Deformation Measurements*, Springer. New York, NY.

M.A. Sutton, N. Li, D.C. Joy, A. P. Reynolds and X. Li, 2007, "Scanning Electron Microscopy for Quantitative Small and Large Deformation Measurements Part I: SEM Imaging at Magnifications from 200 to 10,000," Experimental Mechanics, **47**(6), pp. 775-787.

M.A. Sutton, W.J. Wolters, W.H. Peters, W.F. Ranson and S.R. McNeill, 1983, "Determination of Displacements Using an Improved Digital Correlation Method," Image and Vision Computing, **1(**3), pp. 133-139.

Midwest Optical Systems, n.d., from http://www.midopt.com

North American Stainless Steel, n.d., from http://www.northamericanstainless.com

Point Grey, n.d., from http://www.ptgrey.com

R. Ghorbani, F. Matta and M.A. Sutton, 2015, "Full-Field Deformation Measurement and Crack Mapping on Confined Masonry Walls Using Digital Image Correlation," Experimental Mechanics, **55**(1), pp. 227-243.

S. Mallon, B. Koohbor, A. Kidane and M.A. Sutton, 2015, "Fracture Behavior of Prestressed Composites Subjected to Shock Loading: A DIC-Based Study," Experimental Mechanics, **55**(1), pp. 211-225.

V.P. Rajan, M.N. Rossol and F.W. Zok, 2012, "Optimization of Digital Image Correlation for High-Resolution Strain Mapping of Ceramic Composites," Experimental Mechanics, **52**(9), pp. 1407-1421.

X. Guo, J. Liang, Z. Tang, B. Cao, and M. Yu, 2014, "High-Temperature Digital Image Correlation Method for Full-Field Deformation Measurement Captured with Filters at 2600∘C using Spraying to Form Speckle Patterns," Optical engineering, **53**(6), pp. 063101-1-12.

Yang Y, Li X, Xiao R and Zhang H, 2015, "Digital Image Correlation and Complex Biaxial Loading Tests on Thermal Environment as a Method to Determine the Mechanical Properties of Gh738 using Warm Hydroforming," High Temperature Material Processes, **19**(1), pp. 37-69.